5-2018

Hybrid Energy Storage Systems for UAV Applications

John J. Ganser
Purdue University

HYBRID ENERGY STORAGE SYSTEMS

FOR UAV APPLICATIONS

A Thesis

Submitted to the Faculty

of

Purdue University

by

John J. Ganser

In Partial Fulfillment of the

Requirements for the Degree

of

Master of Science

May 2018

Purdue University

West Lafayette, Indiana

THE PURDUE UNIVERSITY GRADUATE SCHOOL
STATEMENT OF COMMITTEE APPROVAL

Dr. Gozdem Kilaz, Chair

School of Engineering Technology

Dr. Duane D. Dunlap

School of Engineering Technology

Professor Neal Widmer

School of Engineering Technology

Approved by:

Dr. Duane D. Dunlap

Head of the School of Engineering Technology Graduate Program

Dedicated to my wife Jessica, for her unconditional love, support, and encouragement.

ACKNOWLEDGMENTS

I would like to specifically thank my major professor, Prof. Gozdem Kilaz, and Caterpillar mentor Mark Wiley, for encouraging the development of this thesis and providing insight and solutions to technical challenges encountered along the way.

I would also like to thank my wife, Jessica, and the rest of our family for supporting me through this process and the sacrifice of time and resources needed to develop this thesis.

Many other individuals, whom all I could not list here, have helped along the way both personally and professionally. I would like to thank those individuals as well for their tremendous support.

TABLE OF CONTENTS

LIST OF FIGURES

LIST OF TABLES

LIST OF ABBREVIATIONS

ADC	Analog to Digital Converter
Ah	Amp Hour
ANOVA	Analysis of Variance
CFM	Cubic Feet per Minute
CSV	Comma Separated Values
DAC	Digital to Analog Converter
DAQ	Data Acquisition
DC	Direct Current
DEP	Distributed Electric Propulsion
ESR	Equivalent Series Resistance
F	Farad
HESS	Hybrid Energy Storage System
ICE	Internal Combustion Engine
kV	RPM per Volt
mAh	Milliamp Hour
MOSFET	Metal Oxide Semiconductor Field Effect Transistor
PEMFC	Proton Exchange Membrane Fuel Cell
PM	Permanent Magnet
PWM	Pulse Width Modulation
RPM	Revolutions per Minute
SOC	State of Charge
SOH	State of Health
UAS	Unmanned Aerial Systems
UAV	Unmanned Aerial Vehicle
VTOL	Vertical Takeoff and Landing
Wh	Watt Hour

GLOSSARY

Brushless DC Motor	A permanent magnet (PM) motor that converts or produces direct current via the magnetic interaction between the rotor windings and stator magnets (Mi, Masrur, & Gao, 2011, p. 272).
DC-DC Converter	A power electronics component that decouples two direct current (DC) voltages and either raises or lowers the source voltage (Bose, 2014).
Drone	An autonomous or self-controlled unmanned aerial vehicle (UAV) (Leasure & Nolan, 2015, p. 15).
Hybrid Energy Storage System	An energy storage system that combines high power and high energy storage units together (Zimmermann et al., 2016, para. 1).
Parallel Hybrid	The electric motor and internal combustion engine (ICE) both deliver power to the final drive output (Mi et al., 2011, p. 13).
Passive HESS	The "direct parallel connection of two or more different cell technologies"(para. 5). The coupling of cell types "is carried out passively, without use of an intermediary power electronic converter" (Zimmermann et al., 2016, para. 6).
Power Electronics	The conversion and control of electrical power (Bose, 2014, para. 1).
Range Extender	A device that extends the range of an electric vehicle by the incorporation of an ICE to drive the vehicle once the electric power is depleted (Mi et al., 2011, p. 107).

Series Hybrid	The ICE converts chemical energy to mechanical power and the mechanical power is then used to produce electrical power. This electrical power is then used to power separate drive motors directly or stored for later use (Mi et al., 2011, p. 12).
Super and Ultra Capacitors	Electrochemical energy storage device that stores "electrical energy in the form of an electric field between two conducting plates" (Grbovic, 2014, p. 5). The terms ultracapacitor and supercapacitor are synonymous with each other and could be used interchangeably.
Unmanned Aerial Vehicle	The U.S. Department of Defense (2013) defines an unmanned aircraft as an "aircraft or balloon that does not carry human operator and is capable of flight under remote control or autonomous programming" (p. 15).

ABSTRACT

Ganser, John J. M.S., Purdue University, May 2018. Hybrid Energy Storage Systems for UAV Applications. Major Professor: Gozdem Kilaz.

Energy storage constraints limit the range and endurance of electric based unmanned aerial vehicles (UAVs). Solving the energy storage problem allows the adoption of UAVs on a much wider scale. A solution to the problem would ideally retain the significant performance and efficiency benefits of the electric based propulsion system. The contents of this study focused on solving the energy storage problem through research, experiment, and simulation based testing of the application of hybrid energy storage systems (HESS) to existing UAV designs.

A review of literature was done exploring existing and future applications of electric based aircraft propulsion systems. Research was conducted on current energy storage technology limitations and potential hybrid energy storage design solutions. The solution allows bridging the gap to full adoption of electric propulsion.

After extensive research, a passively controlled hybrid battery and supercapacitor configuration was chosen for experimental and simulation based evaluations. The experiment and simulation tested for key battery performance improvements using the HESS and its applicability to UAV designs. Results showed a significant reduction to the peak amperage and peak temperature of the battery under identical load profiles. The experimentally tested passive HESS did not show a reduction in energy consumption, but the active HESS simulation results did. The simulation results showed a theoretical gain of 8.8% for state of charge (SOC) for the battery. Equating the SOC to range improvement, a 10% increase in range was possible for the UAV tested.

CHAPTER 1. INTRODUCTION

The contents of this chapter introduced and defined the main focus for this research. Basic problem identification was addressed through having research questions related to the problem statement. Following the problem statement was a definition of the scope of research, which outlined and defined the limitations and delimitations of the resulting work.

1.1 Research Question

The following two sections below presented the motivational and driving force behind the resultant work of this thesis. The research questions were derived in accordance with the problem statement and the subsequent work of this thesis sought to answer those questions.

1.1.1 Main Question

Could a hybrid battery and supercapacitor combination be successfully applied to a UAV?

1.1.2 Sub-Research Questions

- What would the optimum selection and sizing of the hybrid energy storage system components be relative to the size of the craft and mission criteria?
- How could the efficiency and longevity of the on-board hybrid energy storage system be maximized?
- How could an energy storage system be bench tested for performance?
- What physical factors played a role in providing maximum performance and reliability from a hybrid energy storage system?

1.2 Problem Statement

Pure electric propulsion systems offered triple the overall efficiency and scale tolerant power densities for comparison with conventional combustion based technologies. Electric propulsion also had the benefit of producing zero local emissions. Constraints of energy storage technologies limited the ability to implement purely electric propulsion systems in larger and longer range vehicles. Specifically, the lack of energy density of present 2018 battery technologies limited the available amount of energy that could be realistically stored. Aviation based electric propulsion applications represented the greatest challenge in dealing with the excessive weight of the batteries.

Any added performance gains of the electric motor were quickly lost due to the added weight of the battery. The introduction of brushless motors and higher energy density batteries allowed the development of small and lightweight unmanned aerial vehicles (UAV). Scaling these UAV systems to larger platforms was not possible due to the constraints of battery based energy storage.

Different approaches had been attempted for bridging the gap between electric propulsion and traditional combustion based propulsion systems. Hybrid combinations of the two were utilized to try and do exactly that. Again, weight was a limiting factor, as was the operational complexity of the system.

Battery based energy storage systems had taken advantage of the relative higher energy density of lithium batteries. Compared to hydrocarbon based fuels, the relative energy density of batteries was still low. Problems with excessive discharging and charging of the battery also represented a serious challenge to large scale implementation.

A solution was sought to provide a better and more efficient energy storage system. The ideal solution would outperform present day batteries for terms of not only capacity but also safety, reliability, and cost.

1.3 Scope of Research

The contents of this research focused on understanding how to successfully apply a hybrid energy storage system into a small multirotor UAV. Multiple UAV designs existed,

including fixed wing, multirotor, and tilt-rotor or vertical takeoff and landing (VTOL) designs, a hybrid combination of the two. Only the multirotor design was chosen for study due to the simplicity and relevance. After a thorough review of literature surrounding hybrid energy storage systems, the first focus was to find a UAV multirotor test platform.

Emphasis was placed on finding a commonly flown and open source UAV design. The selected test platform would then be used to test the application of a hybrid energy storage system (HESS) battery and supercapacitor combination.

After finding a UAV test platform, the recorded load profile data was extracted from the selected UAV under a specific flight path. The flight was defined under fixed operating conditions for range and payload capacity. Chapter 3, "Methodologies", defines the exact operating conditions under which the experiment was based on. Once the data was collected and validated it was then used to both experimentally bench test and simulate the various HESS configurations.

The focus of the research evaluated the application of a HESS using the defined load profile and experimental and simulation based tests. A statistical regression analysis was conducted to determine if the experimental HESS in fact added any advantages over the battery by itself. Critical performance values of the battery were examined to make the evaluation.

A critical design and analysis component of the research also dealt with how the HESS was defined in terms of selection and sizing of energy storage components. Several different energy sources were available to be combined into the energy storage system and different options were explored. Weight has always been a constraining variable in propulsion design and to address this, the total UAV weight and energy storage system component weights were evaluated. Volume of the energy storage components were also addressed and compared for the conclusion of the study.

1.4 Assumptions

The assumptions for this research study included:

- Variations in power demand of a UAV could have been unpredictable based on external, ambient based conditions
- Increased payloads could have caused a decrease in efficiency unrelated to the energy storage system
- Costs of various battery and capacitor technologies would limit selection for testing
- Uncontrolled state of charge and ambient conditions could lead to unpredictable test results

1.5 Limitations

The limitations for this research study included:

- Obtain a specific dynamic power profile for a specific UAV, payload, and mission criteria either from a real UAV or from a simulation
- Create a testable energy storage system, consisting of a passively paralleled battery and supercapacitor
- Create a bench configurable testing apparatus that could cycle the power system according to the obtained dynamic power profile
- Run a statistical analysis to determine predictor variables associated with the range and life cycle count
- Test the hypothesis that various HESS configurations improved battery performance, under a specific load, for several different response variables:
  - Battery voltage
  - Battery temperature
  - Battery capacity consumed

  - Battery average current
  - Battery peak current

1.6 Delimitations

The delimitations for this research study included:

- Not testing for differences associated with varying battery chemistries
- Test only the HESS on a bench apparatus and in simulation, and not on an actual UAV
- Results not guaranteed to increase range as much as they were for increasing battery life (life cycle count). The added complexity and efficiency losses from the entire HESS could have caused a wash of performance gains for range

1.7 Summary

Chapter 2 of this study reviewed available literature associated with the topic of electric propulsion, energy constraints, and hybrid energy storage systems. Preliminary answers to the presented research questions and problem statement were sought through a rigorous examination of current and future propulsion technology. The emergent best approach and solution was further derived, examined, and tested for the applicability to UAVs.

CHAPTER 2. REVIEW OF LITERATURE

As technology advanced in the area of power electronics and electric motor design so did the opportunity for its use in a wide variety of applications. Mobile transportation systems had the largest opportunity for electrification due to their tremendous inefficiencies and subsequent harmful localized emissions. Specifically, smaller sized UAVs saw significant performance gains and the ability to implement successful multi-rotor control with electric propulsion technologies.

The main limitation to further adaptation of these electric propulsion systems was for on-board energy storage. Electrical energy storage constraints limited the overall range and payload capacity. Traditional combustion propulsion systems made up the inefficiencies of their power plant by utilizing energy dense, non-renewable based fuels. Increased capacity of on-board electric based energy storage and increased efficiencies of the electric propulsion system would help further develop electric propulsion. Electric propulsion would then replace combustion based propulsion systems as a superior alternative.

The proceeding sections of the literature review provide an insight into current electric aircraft concepts and their need for increased energy storage capacity. Existing hybrid designs and power systems that sought to bridge the gap between combustion and electrification systems were also examined in detail.

Constraints in available energy storage systems, namely batteries, had significantly hindered further development, due to low available energy capacity and long charging intervals. Batteries and other alternatives such as fuel cells, super and ultra-capacitors, and photovoltaics were explored in the energy storage constraints section of this review.

A final solution of solving the on-board energy problem was proposed by using a hybrid configuration of current state-of-the-art energy storage components. Research on hybrid energy storage systems pointed to a way of combining a battery and capacitor into an energy storage system that outperformed current energy storage components by themselves (Zimmermann et al., 2016). Through advanced control techniques and careful selection of lightweight and durable components, this could be potentially applied to UAV power systems.

2.1 Developments and Limitations in Electrified Aircraft

Several Fortune 500 companies such as Amazon, UPS, and Google have explored the idea of introducing UAV systems into their business models. Specific work had previously been explored by these companies on developing unique UAV systems and addressing the limitations needed to be overcome for implementation.

2.1.1 Uber Elevate

The ride sharing company, Uber (2016), had developed a marketable business concept called "Elevate." The concept revolved around the idea of "on-demand...urban air transportation" (Uber, 2016, p. 2). Uber planed on using a fleet of electric vertical takeoff and landing (VTOL) aircraft to offer an on-demand flying taxi service to transport passengers in between different docking stations. The white paper report by Uber and its technical advisors went into four broad categories of focus and detail: vehicle, infrastructure and operations, rider experience, and economics.

Uber cited that over a dozen different companies were developing concept VTOL aircraft, but the closest manned technology of the time was the helicopter (p. 3). Due to the inefficient nature of the helicopter, the VTOL was presented as a better alternative for a ride sharing, taxi based service.

Uber stated specific energy of modern batteries were "insufficient for long-range commutes" (Uber, 2016, p. 4). A specific energy of 400 W-hr/kg and a cost of less than $100/kW-hr was mentioned as a critical runtime performance requirement for the batteries being used. The cited runtime performance and cost did not exist for batteries at the time of this writing.

Not only was runtime performance and cost a factor, but so was the time between charges. The idea of pulse charging was presented and Uber stated achieving rapid charging "is important, if not more important than achieving high specific energy batteries" (Uber, 2016, p. 38).

2.1.2 NASA - Distributed Electric Propulsion (DEP)

A report done in 2016, by researchers on the NASA SCEPTOR flight demonstration project, highlighted the great advantages to the use of electric propulsion systems for aircraft. According to the study, using what the authors referred to as DEP or distributed electric propulsion allowed an aerodynamic advantage to the wing design, drastically reducing energy consumption. The final reported values of energy savings came out to be 4.8 times less energy than a conventional aircraft (Borer et al., 2016, p. 1).

Due to battery limitations, the range of the concept vehicle was limited to short distances. Prior research by the author discussed the limits of battery technology and its energy capacity as having "60-100 times less than equivalent mass in aviation fuels" (Nickol et al., 2016, p. 2). The need for higher specific energy density batteries was evident in this conclusion.

2.2 Commercial Drone Delivery Services

Large delivery and service based companies, such as Amazon, UPS, and Google, had started developing their own UAV based delivery systems (Amazon, 2016; Business Insider, 2017; X, n.d.). Current focuses tended to be on lightweight, short range delivery systems, where current battery technology allowed a cost effective median for these companies to operate under. As these companies expand their drone based delivery services, battery and propulsion system technologies would have to be able to meet the requirements on a much larger scale.

2.2.1 Amazon Prime Air

Amazon (2016) was testing its own drone based delivery systems in the United Kingdom. The prototypes promised to deliver packages in 30 min or less and to carry a package weighing 5 lb or less (Amazon, 2016). Amazon stated the drone based delivery service increased "overall safety and efficiency of the transportation system" (para. 1). Developments of the delivery service were listed as on going in the United States, United Kingdom, Austria, and Israel.

2.2.2 UPS Drone Delivery

Another prominent delivery company, UPS, was making investments into its own drone based delivery system. According to a report by Business Insider (2017), UPS had already successfully completed a drone delivery in Lithia, Florida. The report stated the octo-rotor or eight rotor craft was designed and built in early 2016 and had a payload capacity of 10 lb and could fly for 30 min (para. 2). The company claimed drone delivery had advantages of lower costs in rural areas and could save the company $50 million dollars per year by eliminating one mile from each driver's routes (Business Insider, 2017, para. 4).

2.2.3 Google Delivery Service

Joining the list of ongoing aerial delivery services was Google, under a company named X. Project Wing had developed a goal of "developing automated flight and delivery" (X, n.d., para. 2). The project started in 2014 under the company name Google X. In September of 2016, testing of aerial delivery services was started by the Virginia Tech Mid-Atlantic Aviation Partnership (X, n.d.).

The goal of the project developers was to create a vehicle that could create a "new commerce system that opens up universal access to the sky" (X, n.d., para. 1). No documented performance or results were given.

2.3 Existing Hybridization Work

Different contexts of hybridization were examined for UAV applications. Hybrid terminology throughout the literature often referred to either the combined UAV aerodynamic structures or the combined elements of traditional propulsive power. The following sections reviewed both references and their importance to overall UAV design and efficiency.

2.3.1 Vertical Takeoff and Landing (VTOL)

Researchers from Istanbul's Technical University conducted a study on the commercialization of a hybrid VTOL UAV system. The article highlighted the increasing growth and demand in civilian based UAV architectures and the need for advanced "long endurance" and "high cruise speed" (Ozdemir et al., 2014, p. 371). The term hybrid referred to multiple contexts in this case. The VTOL design was a combination of a fixed wing and a multi-rotor craft (Leasure & Nolan, 2015; Ozdemir et al., 2014). Hybrid could also have referred to a combination of power systems or energy storage systems.

Two variants of the researchers "TURAC" VTOL were introduced. Variant A, that was being discussed in the paper, was a fully electrified aircraft. Variant B, was a future concept of the "TURAC" which planned to incorporate a fuel cell energy storage system. The fuel cell based energy storage allowed "extended hovering time or in turn less battery weight" (Ozdemir et al., 2014, p. 383).

Aerodynamic studies were carried out to size the various components. The researchers specifically noted weight of the battery was especially important in calculating the entire weight of the UAV. The resulting battery pack selected came in at weighing 22 kg (48 lb) of the total 45 kg (99 lb) maximum takeoff weight. A surprising radial range of 35 km (22 mi) carrying a payload of 8 kg (17.6 lb) was able to be achieved from reported results (Ozdemir et al., 2014, p. 392).

2.3.2 Series and Parallel Hybrid Combustion Based Propulsion

Examples of hybridized aircraft propulsion systems were discovered that highlighted an important aspect of overall hybridization efforts. Overall efficiencies and complexity factored into power system design. Combustion based power systems added a level of complexity by themselves and had strict requirements for maintenance and inspection (Leasure & Nolan, 2015, p. 142). Adding additional components further complicated the system and potentially added unneeded weight. A parallel-hybrid system, that provided simultaneous propulsion power and mitigated the excessive weight, was preferred over a series-hybrid system.

2.3.3 Ultra Micro Turbine

The first example of a series hybrid propulsion system examined the findings of Capata, Marino, and Sciubba. Their 2014 experimental study focused on using an ultra micro gas turbine in a series hybrid configuration to power a long endurance UAV. Extensive design and aerodynamic analysis was done to properly size the power system. The proprietary design of a new combustion chamber for a miniaturized gas turbine was developed and further bench tested to analyze performance.

The results of Capata et al. (2014) bench tests came back with dismal results, finding a totally efficiency of the gas turbine to be 6%. The resulting inefficiencies of the scaled gas turbine were due to a brake specific fuel consumption of 840 g/kW-hr (Capata et al., 2014, p. 33). The results highlighted and represented a serious issue with scaling down any type of combustion based power system. As a power system becomes smaller, it generally became less efficient.

2.3.4 Parallel - Four-Stroke, ICE

The second example dealt with a parallel hybrid setup utilizing a four-stroke reciprocating engine with a brushless DC motor, studied by Friedrich and Robertson in 2015. The goal of their study was to find an existing ultralight aircraft that used a traditional gas power plant and repower the propulsion system with a more energy efficient alternative. The existing Bailey V5 200 cc four-stroke engine was to be removed and replaced by a smaller engine. The smaller engine was then combined with an electric motor in a parallel configuration.

Friedrich and Robertson (2015) used an interesting approach to sizing and evaluating the design of the system. Simulink along with X-plane were used by the researchers to develop a simulated model of the aircraft. The simulation allowed them to see exactly how the aircraft would behave under certain mission requirements.

After determining the needed power requirements, new components were selected to provide the propulsive power. A Honda GX160 four-stroke engine and JM1 brushless DC motor were selected as meeting the requirements of the new system. A bench test of each

component was conducted in order to evaluate performance. Performance for the gas engine was given as an efficiency of 24.3% at 4260 rpm with 10.2 Nm of torque and 4.6 kW of power generated (Friedrich & Robertson, 2015, p. 183).

Longevity and reliability of this engine could be a concern with extending performance parameters past what original design specifications intended.

2.3.5 Parallel - Two-Stroke, ICE

A company called Yeair (n.d.) had designed and built a parallel hybrid propulsion quad-rotor prototype. The power was provided in a parallel configuration that utilized two-stroke engines directly coupled with brushless DC motors. The on-board battery pack was used to start the engines and would be charged during flight. The specifications of the craft showed a maximum flight time of 60 min with a maximum payload of 5 kg (11 lb), and a 55 km (34 mi) range (Yeair, n.d.). The total empty weight was listed as 4.9 kg (10.8 lb).

A significant drawback to this type of power plant was in the fact that it used a two-stroke engine to extend range and payload capacity. Two-strokes combine lubricating oil with the fuel, which lead to significant increases in emissions. This point of power plant selection was further clarified in the proceeding UAV design section.

2.3.6 Series - Two-Stroke, ICE

Quaternium (2015) developed their own version of a hybrid quad-rotor, called the Hybrix, pictured in Figure 2.1. The engine was specified as a two-stroke, using 95 octane gasoline with a 4% lubrication blend. The empty weight was listed at 13.5 kg (29.8 lb) and the maximum takeoff weight at 20 kg (44.1 lb), with a payload capacity of 2.5 kg (5.5 lb).

The Hybrix's power system was considered a series hybrid due to the main rotors not directly being driven by the combustion engine. Quaternium (2015) stated a ten-time increase in duration compared to battery operated quad-rotors.

Figure 2.1. Hybrix, a prototype quad-rotor which utilized a series hybrid propulsion configuration (Quaternium, 2015).

2.4 UAV Design

As seen with multiple propulsion system configurations and designs, several UAV types and designs were also available. Understanding common UAV designs was important to further understanding overall performance characteristics. The proceeding section on mission requirements highlighted how important this is when designing a UAV for certain range and payload capacities.

2.4.1 Mission Requirements

Purdue aviation technology Professors Michael Leasure and Michael Nolan in their 2015 book, *Unmanned Aviation System: The Definitive Guide*, presented an overview of aviation systems and specifically multi-rotor technologies. Chapter 2, "Unmanned Aerial Vehicle Design and Construction", discussed mission requirements and how they are some of the most stringent requirements that must be met in a design. According to the authors, mission's requirements "typically define almost every element of a given design" (Leasure & Nolan, 2015, p. 21).

The decision of using a fixed wing design over a multi-rotor design or a combination of both would have to be made. A "hybrid configuration" could also be used to combine the two elements for an optimized and efficient design (Leasure & Nolan, 2015, p. 25). The two authors also went on to make a critical point, "if ultimate performance is the goal,

an airframe, propulsion system, and payload created to complement each other from inception, will likely prove to be the best design" (Leasure & Nolan, 2015, p. 28).

Within Chapter 5, "Powerplant Theory and Operation," the authors continued to discuss different types of propulsion systems and their advantages. Reciprocating internal combustion based four-stroke and two-stroke engines were presented and discussed first, followed with a brief discussion of gas turbine engines. Finally, electric motors, specifically brushless DC motors, were presented at the end of the chapter. Again, the authors stressed the "choice of propulsion" was based on mission requirements (Leasure & Nolan, 2015, p. 125). Based on inherent design, the two-stroke offered more power density due to power being extracted for every single rotation of the crankshaft. For the four-stroke engine, every two rotations of the crankshaft power could be extracted. The two-stroke therefore offered "higher power to weight ratio" engine with less complexity (Leasure & Nolan, 2015, p. 131). A draw back to two-stroke engines were that "lubricating oil must be premixed with the fuel" (Leasure & Nolan, 2015, p. 130). The mixing creates a severe increase in emissions due to the oil not completely burning during the combustion process.

Leasure and Nolan (2015) went on to present the increasing use of electric motors in UAV applications. Based on the use of electronic speed controllers (ESC), brushless DC motors had been able to be used in replacement of brushed DC technology. DC brushless motors were "85-90%" efficient, where DC brushed motors were "75-80%" efficient (Leasure & Nolan, 2015, p. 137). Selection and sizing of the electric motors was another important aspect in the UAV design. A rule of thumb of 50-100 W/lb was given by the authors in selecting the right type of power rating for the motor. Another critical design criteria for electric motor sizing was kV rating or rpms per volt. A low kV number meant "more turns with thinner wire, higher torque and can turn bigger propellers," and a high kV number meant "less turns with thicker wire, higher rpm with a smaller propeller" (Leasure & Nolan, 2015, p. 141).

2.5 Energy Storage Constraints

The Ragone plot in Figure 2.2 depicted how various energy storage technologies fit in terms of power and energy densities. The farther to the upper right corner of the graph, the more desirable the energy source due to the high power and high energy density. Gasoline and hydrogen represented some of the best performers, but careful and thorough consideration had to be given to each type in terms of overall cost, efficiency, and complexity when implemented into a power and propulsion system.

Fuel cells offered comparable energy densities to gasoline, but severely lacked power density. Opposite of fuel cells were conventional capacitors and electrolytic capacitors, which offered very high-power density but lacked in energy density. A more in-depth overview was given in the proceeding sections to batteries, fuel cells, super and ultra capacitors, and photovoltaics and how they could be applied as energy storage median. Addressing each of these areas helped define a suitable energy storage system applicable to a UAV platform.

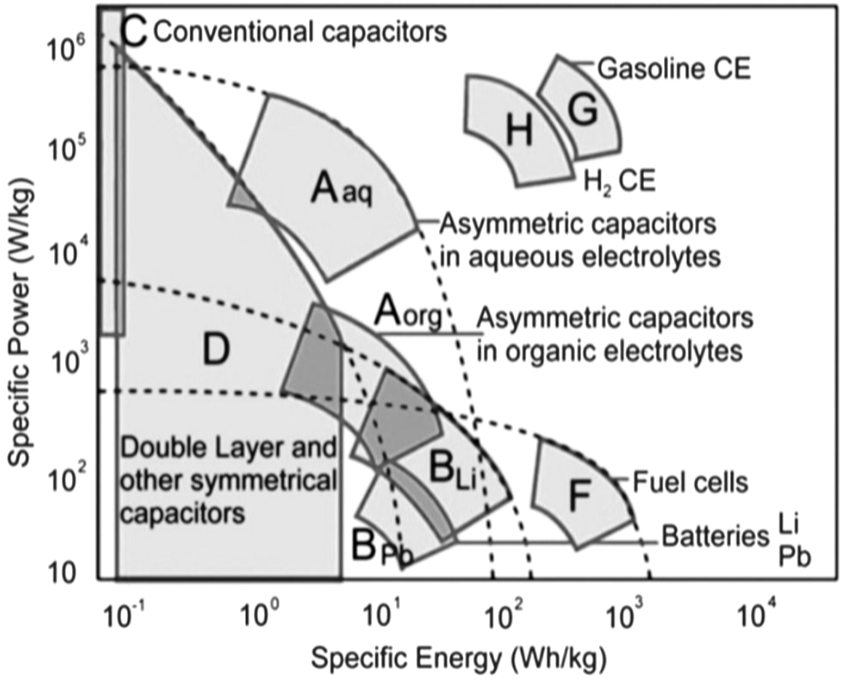

Figure 2.2. Ragone plot of various energy storage technologies, comparing specific power vs. specific energy (Chae et al., 2010; Dubal et al., 2015).

2.5.1 Batteries

Battery technology as an electrical energy storage medium had significantly improved densities with new cathode and anode materials. Despite improvements, the relative low energy density and short life of batteries made them hard to adapt to high energy demand systems.

At the time of this writing, several different types of batteries were available, and more and more research was continuing to be done to investigate increasing overall energy densities. Commonly used batteries included lead acid, lithium ion, and lithium polymer. Lithium based batteries had advanced in terms of thermal management and energy density and were much more stable than when first originally released.

As of 2014, Grbovic cited that current lithium ion and lithium polymer batteries had energy densities of 100-200 Wh/kg with operating cycles of around 500-2000 (p. 17). Traditional lead acid batteries had energy densities of 20-35 Wh/kg and 200-2000 operating cycles (p. 17). The lithium battery technology offered much higher energy density, but still lacked in cycle life. The limitation was especially pronounced if fast charging and discharging were required.

2.5.2 Lithium Batteries and C-Rate

Several different lithium battery chemistries were available at the time of this writing, each with its own advantages and disadvantages. For any lithium chemistry, lithium batteries like to operate in a rather narrow safety window, as shown in Figure 2.3. Charging and discharging at high C-rates would cause the breakdown of internal structures within the battery, limiting the life of the battery.

C-rate established the rate of charge and discharge of the battery. The capacity of the battery, C, was defined typically in amp hours and was how many amps the battery could draw for one hour before being completely depleted. nC related to current draw over or under the standard 1C rate, where the discharge time was 1/n hours (Mi et al., 2011, p. 317). Higher C-rates for both charging and discharging could have different effects between different battery types and chemistries. Less reactive batteries had a higher internal

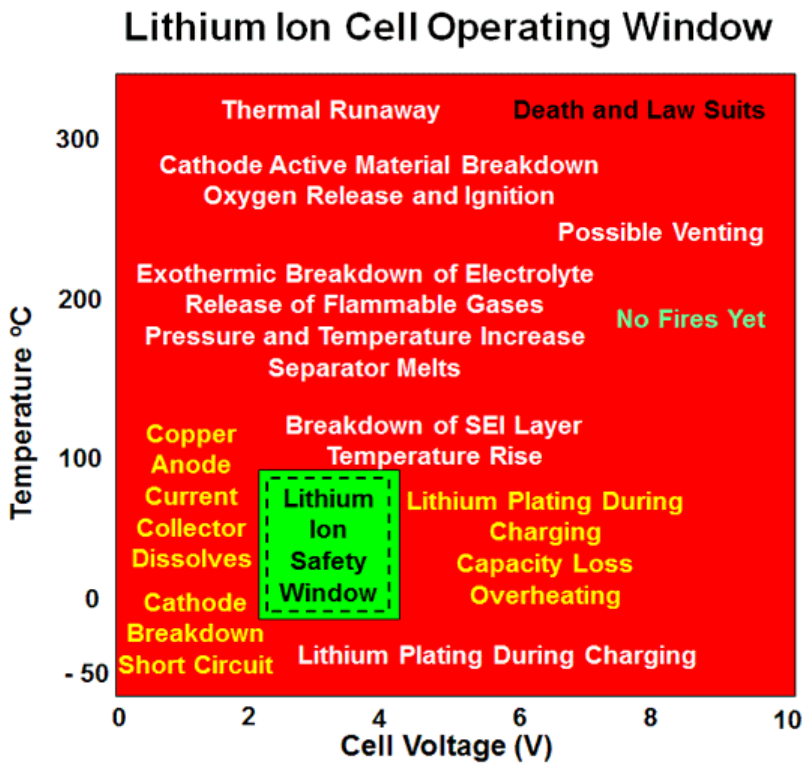

Figure 2.3. Ideal operating window of lithium ion based cells (Electropaedia, 2005).

resistance due to chemical polarizing characteristics. Specifically, ohmic, activation, and concentration polarization factors all played a part in determining the cells internal resistance (Root, 2011).

As a battery was pushed to its performance limits, the internal resistance would become a factor as excessive heat was built up internally due to the I^2R loss. Polarization factors could also cause the voltage level to sag prematurely within the cell under high current draw, causing voltage stabilization issues. Applying lithium batteries to mobile power systems required properly sizing and selecting a battery that could be maintained at a safe C-rate for both charge and discharge situations.

2.5.3 Fuel Cells

Opportunities for storing and obtaining electrical energy were also available for other types of electrochemical energy conversion processes, specifically in the use of fuel

cells. Problems could arise from particular designs of fuel cells, especially concerning volume and weight considerations. Mi, Masrur, and Gao (2011) discussed the basics of fuel cells and the different types available. The most common type was the proton exchange membrane fuel cell (PEMFC), which was favored over other types of fuel cells due to lower operating temperatures of around 80°C (Mi et al., 2011, p. 346).

The major disadvantages of fuel cells were listed by the authors as "high cost, unsatisfactory durability, poor transient performance, and sub-zero temperature startup" (Mi et al., 2011, p. 346). Low power densities of the fuel cells created a situation where high electrical power demand during acceleration could not be fully met by the fuel cell alone. Despite these limitations, the average fuel cell was capable of 60% energy conversion efficiency (Mi et al., 2011, p. 347). A penalty for less than optimum power draws, over or under 25%, led to lowered efficiencies of the fuel cell (Mi et al., 2011, p. 348).

A solution presented by the authors in this case was to combine a fuel cell power system with a battery and or an ultracapacitor. A hybrid controller, using a DC/DC buck boost converter, could optimize the control of the different components in a way that maximized the efficiency of the fuel cells and extended their longevity (Mi et al., 2011, p. 360).

Jensen, Schaltz, Koustrup, and Kaer (2013) discussed some of the fundamentals related to fuel cell hybridization within an electric vehicle and performed simulations of various fuel cell architectures. The authors referred to the "Achilles heel" of electric vehicles as being in the energy storage system. Fuel cells offered a way to extend the range in an electric vehicle, while not having to wait for a battery to recharge (Jensen et al., 2013, p. 51).

Results of the simulated analysis showed that although efficiency gains could be made, a penalty was incurred for going over performance design requirements (Jensen et al., 2013, p. 58). The authors also made the case for the need of better control systems to optimize the operation of the fuel cell itself.

2.5.4 Super and Ultra Capacitors

Traditional capacitors, based on the physical properties of two electrical plates separated by a dielectric, were capable of holding a large electrical charge for temporary energy storage (Grbovic, 2014, p. 3). Capacitors are known to quickly charge and discharge and endure a high life cycle before degrading. A million or more cycles of charging and discharging had been seen in electrochemical based capacitors (Miller & Simon, 2008, para. 6). Capacitors are a form of energy storage known as a direct storage. Capacitors are very efficient due to energy not having to change to another form (Grbovic, 2014). To utilize stored chemical or mechanical energy, energy is lost due to the conversion process.

Capacitors of the electrostatic form were "insufficient for most power conversion applications" (Grbovic, 2014, p. 3). The electrochemical capacitor or ultracapacitor contained two porous electrodes suspended in an electrolyte (Grbovic, 2014, p. 3). The increased surface area, due to the electrolyte, caused a significant increase in capacitance. The increase in capacitance, in turn, allowed much more energy to be stored in the capacitor. Grbovic (2014) gave a comparison of static capacitors to electrochemical capacitors in that the capacitance increased on the order of six magnitudes, leading to "25-60 times the energy capacity" (p. 8).

A promising study of graphene based ultracapacitors in 2013 had revealed an energy density rating of 148.75 Wh/kg in lab testing (Yang et al., 2013, p. 9). The cited range of energy density was close to some high-performance lithium battery technologies on the market.

A limitation of super or ultracapacitors was that while they have very high capacitance, their voltages tended to be lower (Kerns, 2015). Voltage limitations created a challenge when integrating the capacitor into a higher voltage system.

2.5.5 Photovoltaics

Harnessing the power of the sun for energy was a possibility, but technology limitations made it difficult to apply for mobile applications. Low energy conversion rates

were a constraint due to subsequent area and weight requirements, which limited being able to apply this type of power source.

Three types of photovoltaic or solar based cell technology existed: silicon, thin-film, and concentrators (Kurtz, 2010). Thin film applications had a promising solution to mobile applications based on their relative lightweight and flexibility (Kurtz, 2010). Due to thin film's inherent inefficiencies, more surface area would be required to get equivalent power outputs as silicon based solar cells (Kurtz, 2010). The National Renewable Energy Laboratory (NREL) report by Kurtz (2010) highlighted the problem of thin film technology as being linked to moisture contamination and the need for a sealed protective layer of glass on both surfaces of the cell. If this problem could be solved, the application of thin-film based cells could be better utilized.

If surface area and weight constraints could be offset by a large wingspan aircraft, solar power could be used. A prominent example of this was seen in 2016 as the Solar Impulse aircraft completed a record 17-stop, around the world flight without using any fuel other than solar power (Fawzy, 2016). The hybrid electric propulsion system used 17,248 solar cells to recharge four batteries, which then powered four 17.5 hp brushless geared DC motors (Solar Impulse, n.d.).

The major constraint to the solar impulse aircraft was its wing span was 72 m wide, the same as a Boeing 747's wing span (Fawzy, 2016; Solar Impulse, n.d., para. 4). The reason for such a large wing span was due to the inefficiencies of the solar panels. Figure 2.4 showed just how large the wing span actually was.

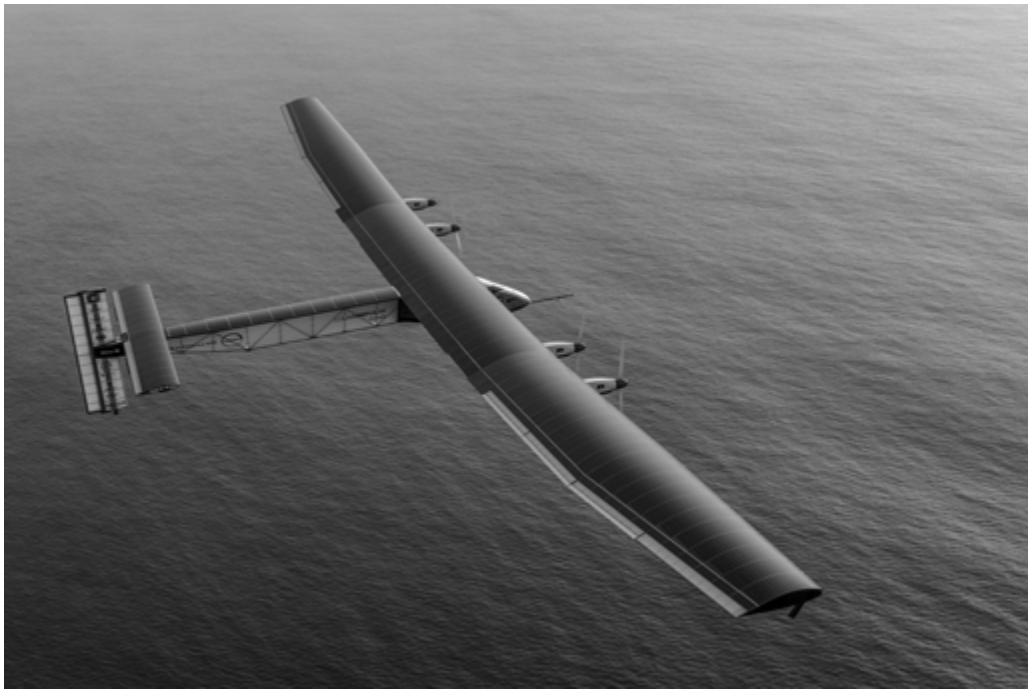

Figure 2.4. Solar Impulse transpacific flight. © Jean Revillard/ Rezo.ch (Solar Impulse, 2016).

2.6 Opportunity for Research and Advancement

Finding the optimum solution to the energy storage problem meant combining existing energy storage technologies together. Research was found in the subject area of vehicle electrification, specifically work pertaining to the hybridization of the energy storage system.

2.6.1 Hybrid Energy Storage Systems

The following two subsections discussed the work surrounding hybrid energy storage systems (HESS) and their application. The first section defined the terminology related to HESS and its topology. The final section discussed research related to the quantitative analysis of the HESS system.

2.6.1.1 Discrete and Modularized HESS

The work done by Zimmermann et al. (2016) discussed and reviewed various hybrid energy storage system (HESS) topologies and added a third major type of topology, the discrete HESS (p. 84). The HESS combined a battery system with a capacitor system to develop an optimum energy performance characteristic by increasing charge and discharge efficiency and increasing longevity of the battery.

According to the researchers, three distinct areas of HESS existed: passive, active, and discrete. Passive HESS directly paralleled the battery with the capacitor. The advantages to this passive system were applicable to what the authors called a "pulsating load" which enabled "higher peak power with lower losses" (Zimmermann et al., 2016, p. 80). The disadvantages of this type of configuration were the operating voltage was limited by the lowest voltage device and "power distribution cannot be influenced" (Zimmermann et al., 2016, p. 80). Compared to the passive HESS, active HESS sought to control the power distribution in a way that helped optimize performance. The two sub categories of active HESS were semi active and full active. The semi active system "decoupled" either the battery or capacitor system from the power load using a DC/DC converter. Full active systems decoupled both battery and capacitor systems in a combination of DC/DC converters.

Despite the complexity of using a DC/DC converter, great increases of range were enabled with advanced control methods. The authors cited research in the area of "PID-based control" as being able to achieve 36.8% increase in range, and "fuzzy sliding mode control" allowed an increase of 42.1% in range (Zimmermann et al., 2016, p. 82).

The third type of HESS was the discrete HESS, which combined "energy storage modules" limited to 60 V per module. The authors cited this as a "voltage class A" restriction, with "reconfigurable cells" (p. 85). The reconfiguration aspect allowed the cells to be connected automatically in different series, parallel, and series-parallel combinations to achieve the desired voltage and amperage.

The researchers pointed out a gap of research in terms of the battery management system as well as the application of the modularized HESS in commercial vehicles and aircraft.

The gap of research represented a stepping stone for further investigating range extending technologies and its applicability to UAV systems.

2.6.1.2 HESS Analytics

Battery and ultracapacitor hybrid configurations had been previously studied and verified for their specific benefits and potential applications. The work by Dougal et al. (2002) established a mathematical relationship to quantify the specific benefits of such a system. The hybrid combination studied by the authors provided three main benefits in pulsed power applications. Peak power of the system was greatly enhanced, energy lost due to heat build-up in the battery was eliminated, and subsequently from the decreased loss of energy in the battery, the battery had a longer discharge time.

Defining the pulse frequency and duty cycle of the load profile determined the magnitude of benefit the hybrid battery ultracapacitor system could give. The research of Dougal et al. (2002) went in depth to define a simple mathematical equivalent circuit model for analysis. A basic resistor and capacitor circuit were used to relate the battery and capacitor, with resistance of each element a critical factor. From the simple equivalent circuit, a "Thevenin equivalent voltage" was derived to analyze the system in the frequency domain (p. 121).

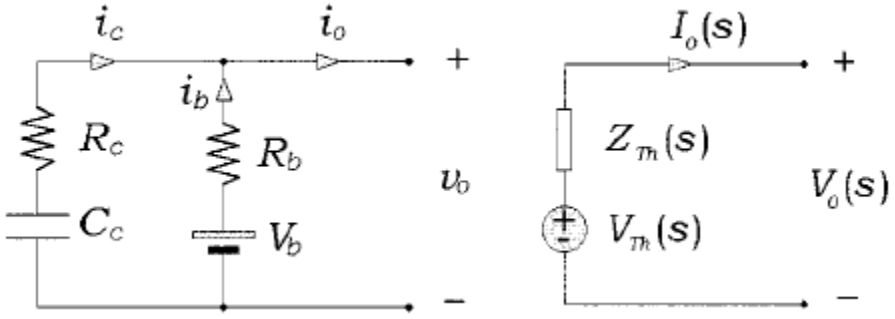

Figure 2.5. Equivalent circuit model of the battery and ultracapacitor, as well as the related Thevenin equivalent circuit (Dougal et al., 2002).

The system frequency, f, and the duty cycle, D, were then used by the researchers to define the current in the frequency domain using the Laplace transform. Solving the Thevenin voltage in the time domain allowed current for each circuit element to be found.

A key take away from the mathematical model was the benefit of the hybrid battery and supercapacitor combination. The benefit was determined by the series-parallel configuration or index of the capacitor array (m). Other factors included duty cycle of the pulsed power (D), the frequency of the pulse (f), and the equivalent series resistance (ESR) of the capacitors (R_c).

Peak power sharing ability was directly related to the ESR of the capacitors (Dougal et al., 2002, p. 123). The peak power enhancement factor, γ, was defined in Equation 2.1. The factor is the result of summing internal resistances of the battery, R_b, and total ESR of the capacitor, R_c. Finally, the result is then divided by the total ESR of the capacitor, holding true as the duty cycle approaches 0. The peak power enhancement factor related to how fast the capacitor could react to the load pulse vs the reaction of the battery. The reactivity also related to an internal loss reduction in the battery, increasing available energy.

$$\gamma = \frac{R_b + R_c}{R_c} \tag{2.1}$$

Internal loss reduction of the battery led to the extension of run time for the battery. A power savings factor, ϵ, was used by the researchers to relate the power lost in the battery by itself to the power lost in the battery and capacitor hybrid. Again, the lower resistance of the capacitor allowed the power pulse to be taken by the capacitor and eliminated a portion of energy lost due to heat dissipation (I^2R). As the frequency of the pulse increased, the power savings directly related to the ratio of internal resistances. The denominator of the equation related the sum of battery internal resistance and the capacitor ESR divided by, m, the series parallel index (Dougal et al., 2002, p. 126). The index, m, was defined by the number of capacitors in parallel divided by the number of capacitors in series. Equation 2.2 showed the function of the power savings factor with relation to the duty cycle, the series parallel index, and the frequency of the system.

$$\epsilon = \frac{P_{i,b} - P_{i,bc}}{P_{i,b}} \Rightarrow \ \epsilon(D,m)(1-D)\frac{R_b}{R_b + \frac{R_c}{m}} \ as \ f \rightarrow \inf \tag{2.2}$$

2.6.1.3 Passive HESS vs Active HESS

A follow up study by Chuan et al. (2012) continued the work of Dougal et al. (2002) and compared the application of passive HESS in electric and hybrid electric vehicles. Due to the simplicity of the passive HESS system, the authors claimed it was more reliable and more efficient than the active HESS system. The active HESS system required a controlled DC-DC conversion, which according to the authors required a complex PWM control as well as an efficiency loss.

The mathematical model derived by Dougal et al. was used as an input into the researchers Matlab Simulink model. Both simulation and experiment were conducted to evaluate the benefits of a passive HESS vs a battery only energy storage system. According to the conclusion of the work, the results of the research showed power capability increased by 2.6 times, discharge time increased by 30%, and energy efficiency increased by 10% (Chuan et al., 2012, p. 89).

Again, the key points derived from this work and that of previous work by Dougal et al. pointed to the importance of resistances of the battery versus resistances of the capacitor. For the capacitor to take on a larger portion of the peak load, it must have a lower resistance than the battery.

2.7 Conclusion of Literature Review

Applications utilizing electric propulsion, specifically in aviation, would continue to grow as the limitations and problems associated with electrical energy storage systems were solved. Large scale transportation and delivery service orientated businesses were already in the planning and development stages of integrating purely electric propulsion into their existing fleets.

Research into the hybridization of aircraft spanned from various overall aerodynamic designs to combining electric and combustion propulsion systems into a single unit. Hybrid systems had been sought after to bridge the gap between the desire to build larger, long range, high payload capable aircraft and the limitations of low energy density electrical energy storage systems.

Opportunities were in the development of the ideal electrical energy storage system. Not one single energy storage technology provided a superior solution in terms of high energy density as well as high power density. Combining various energy storage technologies had the possibility of meeting those idealized needs. Further study was needed to determine if applying a combined hybridized battery and supercapacitor system to a UAV was possible. Insight was also needed for subsequent advantages to overall performance and cost, in contrast to the battery by itself.

CHAPTER 3. RESEARCH METHODOLOGY

The proceeding sections covered details pertaining to the methodologies used in the experimental and simulation based investigation of specific HESS configurations for UAV applications.

The specific research question and hypothesis were defined in terms of the overall intent of the research set forth by this study. Following the hypothesis was an overview of the design of the experiment. Next, a detailed overview was then presented on the development, design, and building of the UAV test platform and the electronic load tester needed for carrying out the experiment.

A comprehensive overview of the HESS system along with supporting circuit diagrams then followed. A detailed overview of the testing conditions, control variables, and procedures were given in exact accordance to how the experiment was carried out. Supporting information on data acquisition including sensing equipment, measurement, and data processing were given as well.

As a validation tool for the collected experimental data, a Matlab R2017a Simulink simulation model was developed and ran for comparison. Details and parameters of the simulation are presented as well.

To conclude the methodologies chapter, success criteria and threats to validity were addressed and defined.

3.1 Research Question

The research question from chapter one was, "could a hybrid battery and supercapacitor combination be successfully applied to a UAV?" The specific research question related to the underlying focus of exploring certain HESS configurations and their applications. The HESS configuration was in reference to a parallel battery and supercapacitor arrangement that was passively controlled and to be used as the primary energy storage system for a UAV.

Successful application of the system focused on the feasibility in terms of performance improvements and constraints relative to the application. Proceeding sections

of the research methodology also defined specific criteria needed to classify the results of the study as being successful or not.

3.2 Hypothesis

To gauge the performance criteria of the HESS configuration, several potential variables were examined to determine statistical significance. Critical parameters of the battery related to state of charge (SOC) and state of health (SOH). Factors specific to the battery included the open circuit voltage, cell temperatures, discharge and charge capacity, average current, and peak current.

The fixed predictor variable was whether or not using a certain passive, paralleled battery and supercapacitor configuration would improve overall performance. The comparison was to the combined energy storage system versus using only the battery system. The testing was carried out under a specific and repeatable current (amperage) profile over the course of a fixed amount of time. Other important control variables were the ambient temperature, type and size of battery, type and size of capacitor, the internal resistance of the battery, the equivalent series resistance (ESR) of the capacitor, and the series-parallel configuration of the battery and supercapacitor.

Specific units of measurement were voltage and amperage for both the main circuit and for the battery and capacitor branches of the circuit. Ambient and battery temperature changes were also recorded. Range or run time improvement was based on the estimated SOC percentage remaining after each test.

The significance level was set to 5% α.

The hypothesis for this study included the following null and alternative hypothesis statements:

H_0: If a certain HESS configuration was used, and important variables were controlled for, then no difference for the resulting battery parameters would be observed between the HESS and the battery system by itself.

H_α: If a certain HESS configuration was used, and important variables were controlled for, then a positive influence would be seen for the resulting battery parameters for the HESS over the battery system by itself.

3.3 Design of Experiment

To test the hypothesis, a basic plan was derived to carry out the experiment. Table 3.1 below shows the testing strategy developed. Controlling the load profile and other important control variables associated with the discharge of the battery allowed the test to be replicated over three different test configurations. One of the test configurations was the battery only, the other two test configurations were two separate HESS configurations.

Five identical lithium polymer batteries were then tested across the three different test configurations. Further details of the experiment, batteries, and HESS configuration were discussed in the proceeding sections of this chapter.

Table 3.1. Experimental design matrix developed for testing purposes.

	Test Configuration		
	Battery Only	HESS-20F5S1P	HESS-80F5S1P
Fixed Load Profile	1 2 3 4 5	1 2 3 4 5	1 2 3 4 5

3.4 Load Profile Selection

The following section contains details of the UAV power system that was subsequently tested. The methodology of the load profile selection as well as the specific configuration and detail of the energy storage system components are listed below.

3.4.1 Design and Build of Small UAV

To gain a better understanding and knowledge of UAV systems, a small sized experimental drone was designed and built. Figure 3.1 showed the finished and working MHQ250 drone. The 250 was a reference to the actual size of the drone, specifically it

referenced the longest distance between propellers, in millimeters. The open source frame design was acquired from Thingiverse.com (2014) and 3D printed with polylactic acid (PLA) filament, a biodegradable plastic. Printing the drone frame allowed for ease of rapid prototyping and quick replacement of damaged components. A key design point integrated

Figure 3.1. MHQ250 drone designed and built for experimental purposes. Original frame design sourced from Thingiverse.com (2014).

into the drone was the autonomous functionality. The 3DR Pixhawk Mini flight controller was selected as the central computer for the drone, offering the benefit of full autonomous control, including automated takeoff, automated way-point to way-point flight, and automated landing. The Pixhawk flight control platform also allowed full data logging capabilities for voltage, current, and control surfaces throughout the entire flight.

3.4.2 Flight Path Analysis and Selection

The selected load profile was based on real data from an actual recorded multi-rotor flight. The load was characterized by a time series of varying currents, as recorded by the

flight controller current sensor. Analyzing the flight log data revealed current was recorded at a sampling rate of 3 Hz, which equated to a current measurement approximately every 1/3 s. The duration and amplitude of the flight path were based off what was within limits of the selected batteries capacity. For experimental purposes, it was assumed the bench test setup would be able to accurately and precisely replicate the load experienced during the actual flight. Post validation was done to assure this assumption was held correctly.

3.4.2.1 Final Selected Load Profile

The actual flight path chosen for testing purposes was based off a publicly shared flight log of another drone and not of the MHQ flight data. Investigation into the MHQ's current (amperage) plots revealed a miscalibration of the current sensor and subsequent recorded flight log data. Public flight logs were available for download from the PX4 (Pixhawk) flight review website (https://review.px4.io).

Recorded data was found for a DJI Flamewheel 450 drone, with a flight time of 4 min and 53 s, and a total energy consumption of approximately 945 mAh. For purposes of testing and simplicity, the flight path was chosen based on the approximate amplitude and pulse rate of the flight path. The maximum current recorded was 17.24 A and the average current was 11.57 A. A 2 min rest period was added to the end of the flight path profile to give time for the battery and capacitor to come to a steady state, which enabled the capture of consist voltage measurements. The exact flight load profile was shown on the following page in Figure 3.2.

3.5 Experimental Equipment Design

To test the effectiveness of the various HESS configurations, equipment had to be sourced that could accurately and precisely replicate the load. Such battery testing equipment, which could be programmed for a specific discharge profile at the required power level, was not readily available. To get the equipment required to complete the testing, a special purpose bench test system was designed and built.

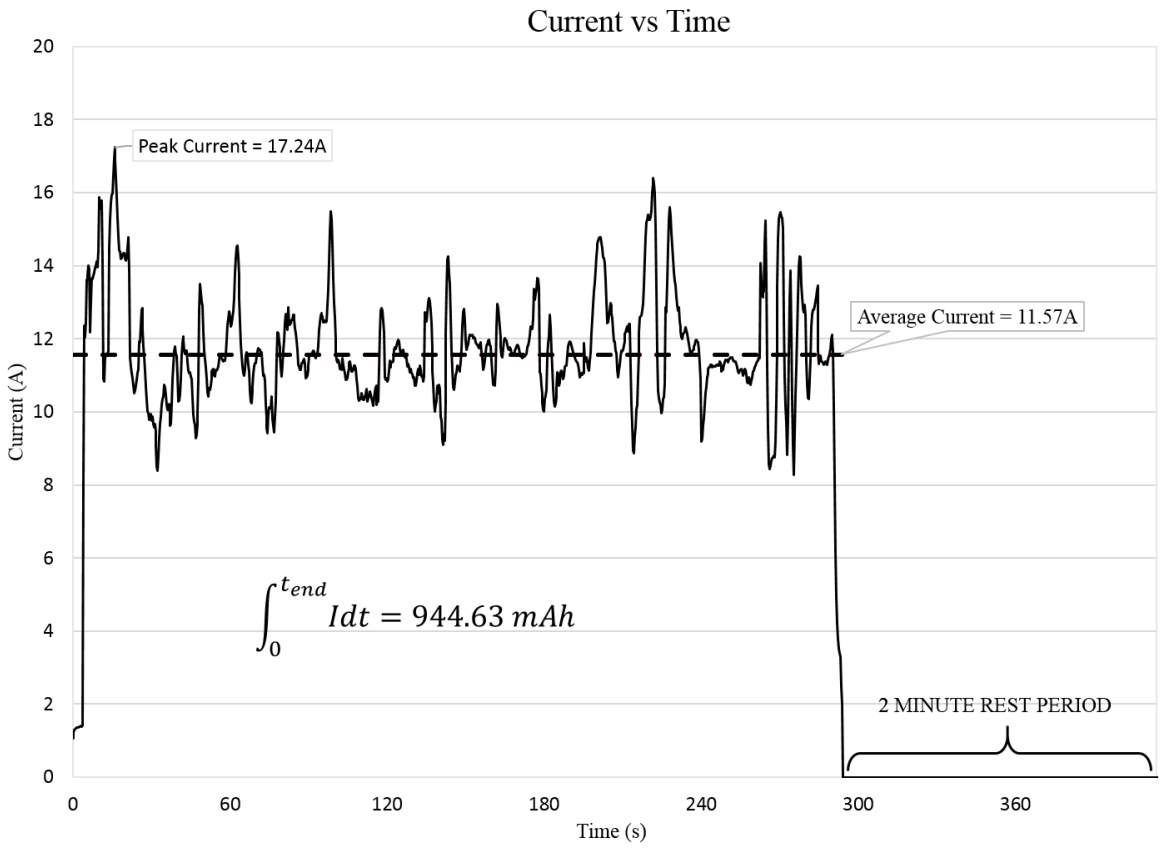

Figure 3.2. Load profile selected for testing purposes. Total flight time was 4 min and 53 s. The total energy consumed was approximately 944 mAh. Plot developed with Microsoft Excel 2016.

3.5.1 Design and Build of Electronic Load Test

A bench test was purposely designed and built for carrying out the experiment. The final design and setup was shown in Figure 3.3. The battery and 20F5S1P supercapacitor array were shown connected in parallel to the input of the tester.

The design was conceptually based off the work of Sikken (2014). The original design was only capable of handling only a peak of 5 A and 30 W, so scaling of the design had to be done to operate within the required power window. The selected load profile for testing had a peak of approximately 17 A and an equivalent average power draw of around 140 W.

To allow such an increase in load from the original design, a specific, high performance MOSFET was used in parallel. The IXYS IXTN200N10L2 MOSFET was chosen for its rating of 178 A and 830 W maximum power dissipation. The technical

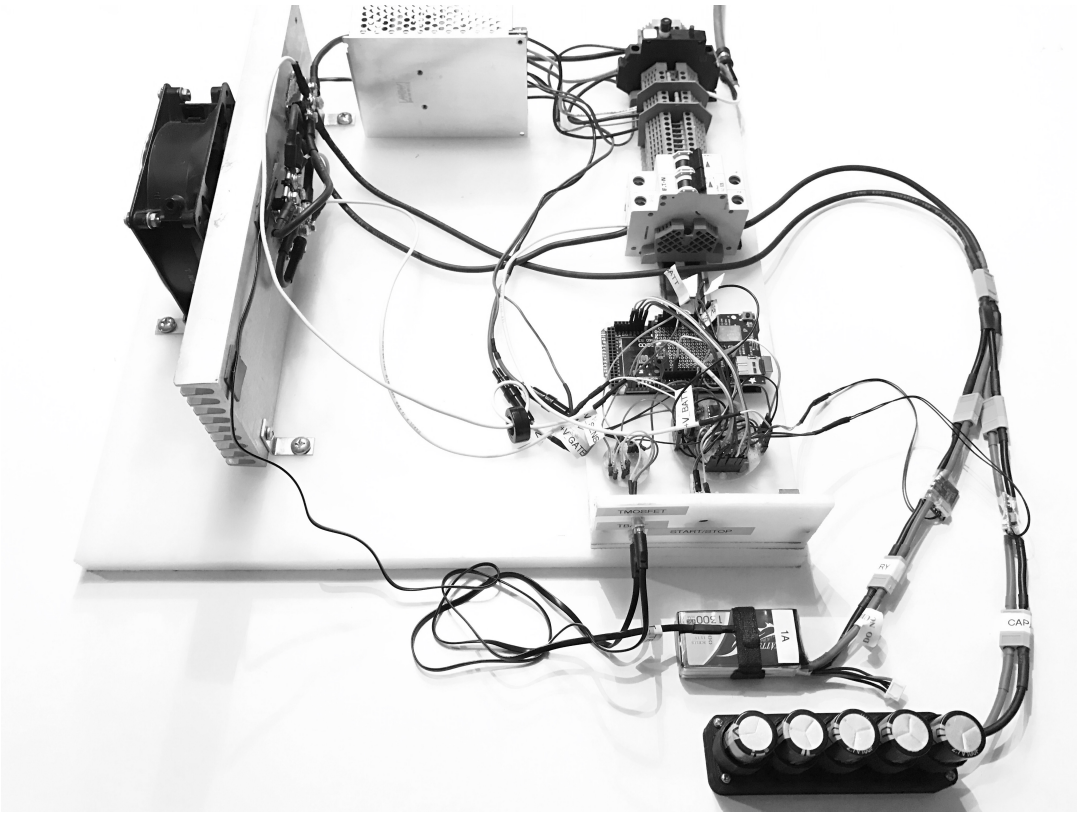

Figure 3.3. Electronic load bench test apparatus developed for testing the HESS configuration. Reference Appendix A for complete circuit diagram.

literature for the MOSFET limits the temperature of the junction to 150°C. Page 5, Figure 13 of the MOSFET's technical data sheet limits constant current to 80 A at 25°C (IXYS, 2017). The IXYS MOSFET array gave the circuit the ability to handle approximately 160 A peak at 12 V. A design margin of 60% of peak amperage realistically limited peak current to around 100 A.

A complete circuit diagram of the final design could be found in Appendix A. A sample of the programming code developed for the electronic load tester could also be found in Appendix B.

Handling of such high power and currents also required maintaining the cited thermal limits of the MOSFET. A large aluminum finned heat sink with a 102 CFM cooling fan was used to provide adequate heat dissipation. Figure 3.4 shows a close-up image of the installed MOSFETs and current shunt on the heat sink. A 10 kΩ thermistor,

shown atop the MOSFET array, was used to account and control for the temperature dependency of the MOSFETs.

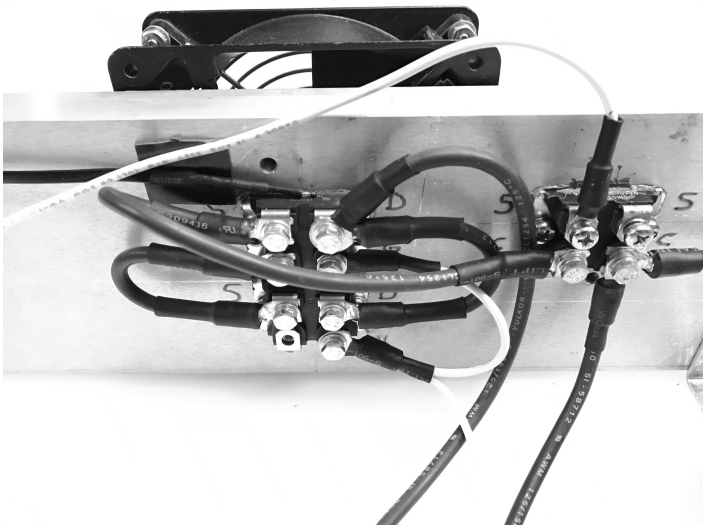

Figure 3.4. Close up image of MOSFET array (left-center) and main current shunt (right). Both devices were mounted to a large aluminum heatsink.

3.5.2 Sensing Equipment

The main measurements required from the test equipment were voltage, current, and temperature. A mix of on board and off board sensing equipment was used to collect the required data.

3.5.2.1 On-Board Sensing

The main circuit of the test equipment included separate main voltage and main current test points. The main voltage was obtained from the positive output of the main breaker, using a basic voltage divider circuit to reduced voltage to below 3.3 V for input into the microcontroller. The current was obtained by employing a 0.01 Ω current shunt in series with the negative side of the main circuit, specifically the low side of the load. The use of selective resistors and capacitors were used to filter excessive noise from the sensors

signals. Operational amplifiers were used for amplifying the voltage signal coming from the current sensor. The amplified signals were then fed into the microcontroller.

3.5.2.2 Off-Board Sensing

Two separate power modules, based off the same sensor used for the Pixhawk and Ardupilot flight controller systems, were used to measure both voltage and current of the battery and supercapacitor branches of the parallel circuit. The power modules were breakout boards that had their own built in voltage divider and current shunt (0.005 Ω) circuits. Another operational amplifier was used to act as a voltage follower and buffer the voltage signals into the microcontroller.

3.6 Energy Storage System Details

The following section contains details pertaining to the selection and design of the individual energy storage components used during the experiment. Specifically, detail was focused on the batteries and supercapacitors used for the test.

3.6.1 Battery Only Configuration

The particular battery selected for testing was a basic lithium polymer 3S1P 1300 mAh capacity battery with a 45C rating. The 3S1P reference specified the number of individual lithium cells in series-parallel configuration. The nominal voltage rating of the individual cells was 3.7 V, and in a series of three this became 11.1 V. The maximum voltage of each individual cell was 4.2 V, and in series this became 12.6 V. Clear documentation could not be found specifying the exact chemistry used in these particular batteries. Five new batteries of this type were used exclusively for testing. Figure 3.5 on the following page showed the batteries laid out side by side, with a quarter shown for size reference.

The batteries arrived charged at a SOC of 50%. After initially charging the batteries at 1C, a test of internal resistance of the battery showed an average resistance of 13 mΩ.

Figure 3.5. Brand new 1300 mAh, 3S1P, 45C rated lithium polymer batteries used in the experiment.

3.6.2 HESS Configuration

The two HESS configurations tested both consisted of a battery and supercapacitor array in parallel. The arrangement was referred to as a passively controlled HESS, as defined by Zimmermann et al. (2016). The passive control methodology simplified the circuit by minimizing the required components needed. The passive circuit diagram was shown in Figure 3.6. HP1 referred to the capacitor or high-power device and HE1 referred to the battery or high-energy device. The two different supercapacitor configurations tested were custom built 20F5S1P and 80F5S1P arrays. The 5S1P was a reference to the series-parallel configuration of the array. The reason there were five capacitors in series was due to the fact the maximum voltage of available supercapacitors was low (2.7 V for both capacitors used). To keep the supercapacitors within a safe operating window, the supercapacitors had to be able to handle the peak bus voltage of 12.6 V. The series

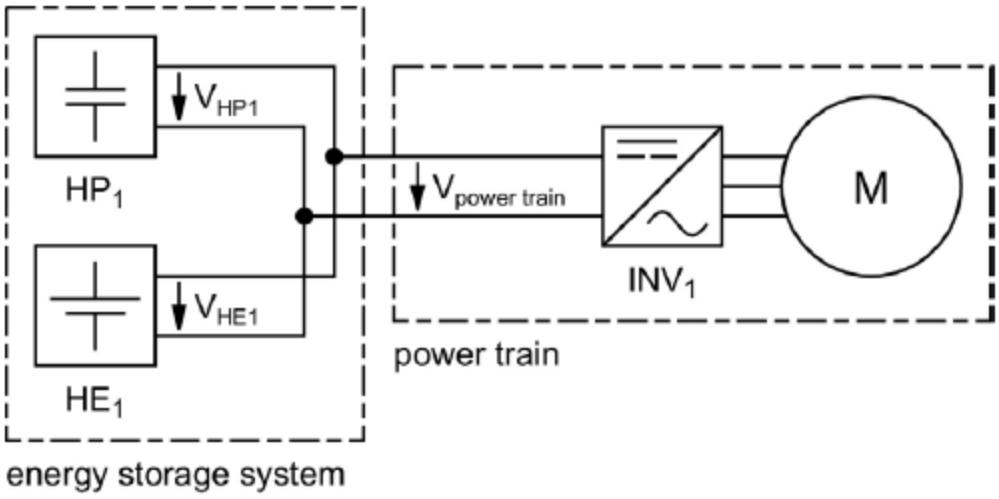

Figure 3.6. Passively controlled HESS configuration (Zimmermann et al., 2016).

configuration put the maximum voltage of the supercapacitors at 13.5 V. The simple summation for this was shown in Equation 3.1 below.

$$V_{Max} = \sum_{i=1}^{n_{Series}} V_{CapRated} \tag{3.1}$$

Adding supercapacitors in series decreased the total capacitance. As shown in Equation 3.2, the resulting capacitance of the array was the quotient of the inverse divided by the sum of the inverses.

$$C_{Array} = \frac{1}{\sum_{i=1}^{n_{Series}} \frac{1}{C_{Rated}}} \tag{3.2}$$

Figure 3.7 showed a very basic and simplified circuit diagram of the actual test configuration and test points used in the experiment. The supercapacitor array was shown as a single capacitor and in Figure 3.8, a more detailed circuit diagram was shown for the supercapacitor array.

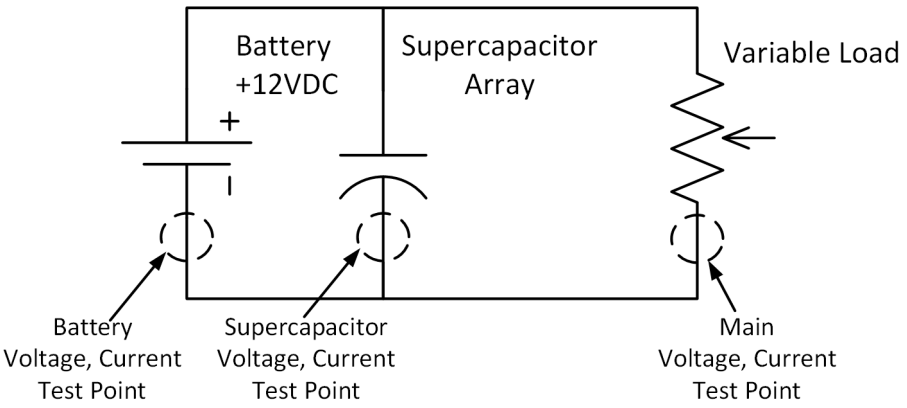

Figure 3.7. Simplified and annotated circuit diagram of the passive HESS configuration. The circuit diagram shown was developed using Visio Professional 2013.

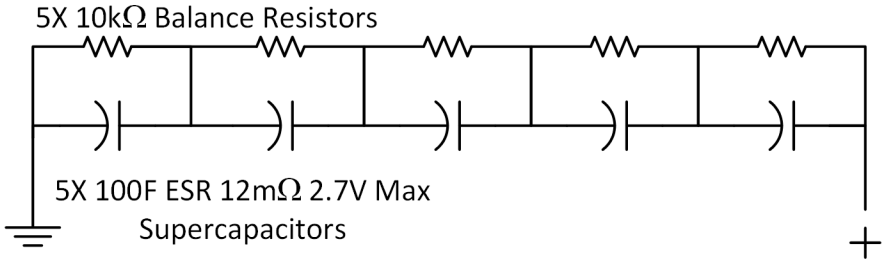

Figure 3.8. Detailed circuit diagram of 20F5S1P supercapacitor array. The circuit diagram shown was developed using Visio Professional 2013.

3.6.2.1 20F5S1P Supercapacitor Array

The 20F5S1P array consisted of five Illinois Capacitor 100 F supercapacitors in series. The equivalent series resistance (ESR) of the individual capacitors was 12 mΩ, summing to a ESR_{Total} of 60 mΩ in series. The calculation of ESR_{Total} was shown in Equation 3.3.

$$ESR_{Total} = \sum_{i=1}^{n_{Series}} ESR_{Rated} \tag{3.3}$$

Five 10 kΩ balance resistors were used to keep the level of charge for each capacitor balanced, eliminating the chance of a high voltage differential across a particular cell.

3.6.2.2 80F5S1P Supercapacitor Array

The 80F5S1P array consisted of five AVX 400 F supercapacitors in series. The ESR of the individual capacitors was 2.2 mΩ, summing the individual ESR's results to a ESR_{Total} of 11 mΩ. The AVX 400 F capacitor was chosen for its capacitance rating and the lower ESR value for associated load sharing functionality. These particular capacitors were significantly larger in volume than the 100 F Illinois Capacitors. An image of the finished arrays was shown in Figure 3.9.

Five 470 Ω balance resistors were used to balance each capacitor in the array.

Figure 3.9. 80F5S1P and 20F5S1P supercapacitor arrays purposely built for the experimental test. The smaller sized configuration was the 20F5S1P supercapacitor array. A quarter was shown for size reference.

3.7 Testing Conditions and Control Variables

Important control variables, specific to this test and preliminarily defined in the hypothesis, were the load profile and the starting conditions of the battery and supercapacitor. The expectation was that the load was consistent and exposed the energy

storage components to the same current over each consecutive test. The battery and supercapacitor, for replication of identical conditions for each test, were recharged to a certain voltage level before each test was conducted. The time interval of each consecutive test was aimed at being done within less than one hour.

3.7.1 Load Replication and Validation

A critical control variable associated with this experiment was the load profile programmed into the electronic load tester. The load profile would be replicated the same for each discharge test. Several prior calibration runs had to be obtained to tune in the electronic load tester. Post validation of current deviation was done for each test.

The test apparatus was initially calibrated using a third order polynomial curve fit of the input admittance plot on Figure 7 of the IXYS technical data sheet (IXYS, 2017). A closed loop, temperature feedback control was implemented to account for the thermal drift of the silicon in the MOSFET. As the MOSFET drifted from normal ambient temperature, the resistance value changed across the drain to source, causing changes to the output curve. Correcting for temperature allowed the output current to closely match the commanded current.

A regulated 12 V, 30 A power supply was used as reference for calibration. Five consecutive runs of the load test revealed an average standard deviation of recorded current during discharge being ±52 mA, with the highest standard deviation being ±237 mA and only occurring at one data point during the entire discharge interval.

3.7.2 Ambient Temperature

The location of the test allowed a stable ambient temperature of approximately 21°C (69.8°F).

3.7.3 Battery Voltage

Battery voltage was maintained by consistently charging the batteries to a full 12.6 V and at a 1C charge rate. A secondary validation of battery voltage, before and after each test, was carried out using a battery smart meter from Tenergy.

3.7.4 Capacitor Voltage

Careful control of the supercapacitor array voltage was carried out as well. Immediately after precharging the supercapacitor array, the open circuit voltage of each capacitor array was recorded before each test using a Fluke 376 FC multimeter. Leakage of current out of the 80F5S1P supercapacitor array occurred at a faster rate than the 20F5S1P array. To reduce the leakage of current, time between precharging and discharging had to be limited to less than an hour interval.

3.8 Testing Procedures

The discharge testing was conducted on the electronic load tester, which was designed to replicate the exact load profile programmed into the testing apparatus. As identified in the design of experiment, both the battery by itself and the battery, paralleled with the supercapacitor, were tested under the same identical load profile. The testing cycle commenced after fully charging all batteries. The three main configurations of battery only, 20F5S1P HESS configuration, and 80F5S1P HESS configuration were individually tested in a randomized order. The testing proceeded according to the developed test log. The test log was used to record important test data before, during, and after each test. A copy of the test log data could be found in Appendix C.

Data acquisition (DAQ) and sensing equipment were used to collect voltage, current, and temperature measurements during the experiment. A programmable microcontroller, the Arduino Mega 2560, was used as both the control and DAQ system for the electronic load tester. Once the test was started, the microcontroller output a preprocessed voltage to the gate through a digital to analog converter (DAC), commanding a specific current flow across the paralleled MOSFETs. Simultaneously, the microcontroller processed the

incoming data via an analog to digital converter (ADC). The desired measurements were then output and streamed over a serial USB interface to a connected monitoring computer.

3.8.1 Charging of Supercapacitor Array

Each supercapacitor array was precharged with a separate, non-experimental battery before the start of each test. The reasoning behind using this method was the fact that the supercapacitor would be charged with a separate source from the main battery in a real charging application, so the same was done for the experiment.

The precharging was completed by connecting the supercapacitor in series with another set of 2200 mAh 3S lithium polymer batteries. A 2 Ω inrush limiter was used to limit the spike in current experienced when first connecting the supercapacitor array. After a period of approximately 10 minutes, the supercapacitor array was disconnected from the battery and the voltage of the array was checked and recorded in the test log. The discharge test proceeded immediately after precharging to eliminate premature discharge through the leakage of current from the capacitor array.

3.8.2 Charging of Battery

The batteries were limited to a charge rate of 1C (1300 mA) to avoid premature damage and skewing of any charging data over the course of the experiment. The charging was done in the same room as which the experiment was carried out, allowing the temperature to be closely maintained at a constant temperature. To eliminate as much residual leakage of energy after charging, time between charging and discharging of the battery was reduced as much as possible. Time for recharging each battery took approximately an hour and contributed to the delay between tests.

3.8.3 Discharging Technique and Handling

The actual testing procedure followed an automated discharge process once connected and started on the electronic load tester. The first step in starting the test

procedure involved connecting a computer to the microcontroller via a USB cable and opening the serial monitor in the Arduino IDE 1.8.4 interface. A prompt in the serial monitor acknowledged the connection was made and loading of the discharge profile was completed. Second, the electronic load tester's main power supply was turned on. Third, the connection of the energy storage system was made. Two separate XT60 connectors connected the battery and the supercapacitor in parallel to the main load tester. Only the battery was connected for the battery only test. The fourth and final step to starting the test was flipping the main circuit breaker to the on position and pressing the start/stop button located on the front of the electronic load tester.

After the test was started, an automated data stream of recorded measurements and elapsed time could be seen from the serial monitor of the computer. The test proceeded according to the programmed load profile. The actual discharge portion proceeded for 4 min and 53 s. A programmed 2 min rest period proceeded directly after the discharging completed. The rest period allowed the battery and capacitor voltages to stabilize, while still recording the output data. The rest period put the entire test duration at 6 min and 53 s. After the test was completed, the battery and supercapacitor were disconnected, and the next test proceeded according to the test log.

3.8.4 Data Output

After each test, the data captured in the serial monitor of the computer was copied into a text file, saved as a CSV file type, and archived. The CSV file was later converted over to an XLSX file type to allow for the uploading of the data into Matlab R2017a for post processing and analysis of the results. A sample of raw test data collected could be found in Appendix C.

3.8.5 Preprocessing and Post-Processing of Data

To successfully carry out the experiment, input and output data had to be both preprocessed and post-processed. Both the electronic load tester and the post analysis

Matlab R2017a script required specifically formatted data. A sample of the post-processing Matlab R2017a code can be found in Appendix B.

3.8.5.1 Preprocessing

The selected flight data was first downloaded from the PX4 flight review website (https://review.px4.io/) as a PX4 specific microlog file. The microlog file was then converted into a readable CSV file using a Python based program called Pyulog (2017). Out of the resulting 26 sub CSV files, the "battery_status" file was opened and the "current_filtered_a" column was extracted.

The acquired current profile was then preprocessed and translated to a corresponding gate voltage to match the required input of the electronic load tester. The resulting gate voltage was found by solving a third order polynomial equation matched to the calibrated output of the electric load tester. Finally, the preprocessed load profile data was saved to a microSD card as a CSV file and inserted into the microcontroller for reading.

3.8.5.2 Post-Processing

After completion of each test, the resulting serial monitor data was copied into a specific CSV output file. The file was later converted over to an XLSX file for post-processing. A Matlab R2017a based script was used to analyze and convert the data into a formatted graphical output. From the resulting output, data was transposed to the test log.

3.9 Data Measurement

Measurements of voltage, amperage, and temperature were collected at a sampling rate of 3 Hz to coincide with the discharge profile. These measurements were collected using redundant sensing equipment within the testing circuit.

The goal of the data collection process was to be able to automatically log the data, thus simplifying the process and eliminating the possibility of user error.

3.9.1 Voltage

The voltage was measured at three different points of the circuit. Built into the main electronic load test circuit was a measurement of voltage at the positive lead. The positive lead was located just after the main circuit breaker. Both the battery and supercapacitor branch voltages were also measured using the connected power modules.

3.9.2 Current

Current was measured at three different points of the circuit as well. The main current was measured using a power shunt on the negative or low side of the main circuit, between the MOSFET source and the ground bus. Both the battery and supercapacitor branch currents were also measured using the connected power modules.

3.9.3 Temperature

Temperature was recorded for both the main MOSFET array and the battery using 10 kΩ thermistors. The MOSFET thermistor was permanently fixed to the top MOSFET's junction. The battery thermistor was secured to the outside of the battery pack using a removable Velcro strap.

3.9.4 Energy Consumed

Energy savings calculations were a very important metric to the research. Two methods were employed to try and capture a measurement of energy consumed during the test. The following two sections discussed those methods.

3.9.4.1 Charger Based

The energy put back into the battery after completion of the test was recorded from the battery charger. Energy taken out of the battery must have also equaled how

much energy must have been put back in on recharge. The logic was based on the fact that the charger brought the battery back to the same voltage level after each recharge cycle.

3.9.4.2 Matlab Based

The battery current measurement recorded over the course of the test was used to calculate theoretical energy consumed by the battery. Matlab R2017a was used to post-process the test data and automatically calculate the integral over the course of the discharge test.

3.10 Simulation

For validation purposes, a simulated test of the same load profile used for the experiment was conducted using a Matlab R2017a Simulink model of the same battery only and HESS configurations. The simulation was based off the work of Chuan et al. (2012), in which a replicated simulation model of the HESS configuration was used. The simulation model allowed testing of not only the passive HESS configurations but also other active and semi active HESS configurations. A sample of the code used to initialize and run the simulation could be found in Appendix B.

3.10.1 Simulation Model

Figure 3.10 showed the exact setup of the simulation model within Matlab R2017a Simulink. The battery and supercapacitor were connected in a passive parallel arrangement. Simscape Power Systems add-in was specifically used for the predefined battery and supercapacitor blocks. Through the controlled current source block, the identical load profile from the experiment was used as the input load to the simulation. Computed voltage, current, and temperature data from the battery and supercapacitor blocks were then fed to the Matlab R2017a workspace for further processing. The energy consumption was calculated for each branch of the circuit by monitoring the current flow and integrating using a continuous integral block. A script was written to post-process the

acquired simulation data and automatically generate detailed output plots for further analysis.

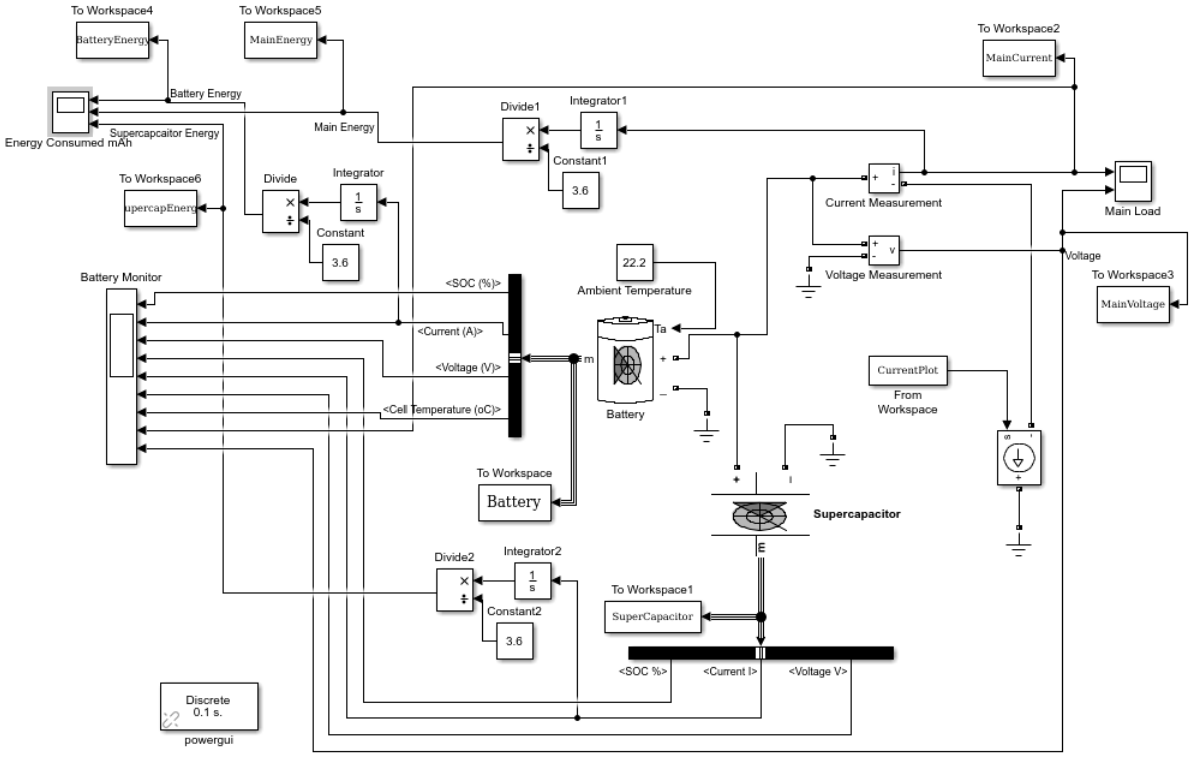

Figure 3.10. Simulink model of HESS developed in Matlab R2017a Simulink. The simulation model was conceptually based off the work of Chuan et al. (2012).

3.10.2 Simulation Parameters

The supercapacitor block parameters were programmatically set using a written Matlab m-script. The block parameters allowed the number of supercapacitors in series and in parallel to be set. Also set was the capacitance of each cell, rated ESR, and starting voltage. The battery block parameters were statically set within the model. Under the battery parameters tab, the battery type was selected as lithium ion and nominal voltage was set to 11.1 V, capacity to 1300 mAh, and starting SOC to 100%. The simulate temperature effects radio button was also selected and the ambient temperature input was selected as 22.2°C (72.5°F). Under the battery discharge tab, the nominal fully charged

voltage was overridden and set to 12.6 V to match with the experimental battery. The simulation solver was set as discrete and the sample time to 0.1 s.

3.11 Defining Criteria of Success

Once the data was collected and compiled from the test log, a statistical analysis was performed to investigate the results of the recorded data. If enough experimental evidence could be shown to support it, it could be concluded to reject the null hypothesis. The confidence level was set to 95% and statistical evidence would support rejecting or accepting the null hypothesis at this level. The confidence level was determined based on the observational nature of the experiment and limited prior data.

Rejecting the null hypothesis would prove an improvement of critical battery performance versus just the battery by itself. The HESS system could then be validated for successful application to a UAV's propulsion system.

3.12 Threats to Validity

Collected experimental data was checked for basic statistical significance assumptions, which included the check of independent observations, equal variance, normality of the data, and linearity. Data was collected according to the defined test conditions and procedures. Automated testing practices were used to eliminate the chance of operator error during data collection.

Standard practice employed for the electronic load circuit design was to use a maximum 1% resistor tolerance. Voltage divider resistor tolerances used in the circuit were rated for 5%, making the rated resistance susceptible to temperature related drifts. Redundant data collection practices were used to counter act this variance and validate the accuracy and precision of the resulting output data.

The overall effect on flight performance due to the increased weight and volume of the added HESS components was not assessed. The purpose of this experimental work was to initially gauge the HESS performance on an observational and exploratory level. At a minimum, to understand the overall impact on flight performance, the proceeding results

section documented and discussed the added HESS weight as a percentage of the total UAV weight. Further real flight testing would need to be conducted to assess and validate the performance gain of the HESS system under real flight conditions.

CHAPTER 4. RESULTS

Contained in the proceeding sections were the results of the experiment and simulation. The results were derived using the methodologies outlined in Chapter 3. The first section of this chapter covered the statistical analysis of the experiment, covering the individual statistical response results. The second section covered results found using the simulation model.

4.1 Experimental Results

The following experimental results were based off 15 test observations, as followed by the design of experiment. The experiment replicated a fixed discharge pattern over the course of these 15 test observations. The observations were divided into thirds and each of three specific test configurations were run five times, in a randomized order.

Several measurements were taken and recorded for each observation carried out on the electronic load tester. Statistical software was then used to analyze the data after completion of testing and recording of all data. Appendix C contained the data recorded in the test log and a sample of raw experimental data.

4.1.1 Statistical Analysis of Experimental Results

The following statistical analysis was carried out using SAS 9.4 and in conjunction with Purdue Statistical Consulting Services. Basic statistical assumptions of independent observations, equal variance, normality, and linearity were met and verified using visual fit diagnostics.

4.1.1.1 Individual Responses

The results contained in Table 4.1 summarized the individual response variables significance with respect to the presence of the HESS configuration during discharge testing. The statistical test was a one-way ANOVA, done 6 separate times. The 6

individual response variables tested were primary indicators of battery performance. Using a significance value of α= 5%, 3 out of the 6 response variables tested were proved to be statistically significant with the use of the HESS system. The null hypothesis could be rejected for those 3 response variables.

Specifically, batt_tempC_peak, batt_tempC_end, and batt_amps_peak response variables were all found to be statistically significant. Out of these 3 significant variables, batt_amps_peak was most significant and batt_tempC_end was least significant.

Response variables not significant were main_volts_end, batt_mAh_charger, and batt_amps_average. The null hypothesis failed to be rejected for these variables.

Table 4.1. Experimental results of the individual response variables statistical significance. The test configuration was used as the predictor variable.

Response Variable	R^2	F Value	Pr>F
main_volts_end	0.07	0.46	0.6410
batt_tempC_peak	0.54	6.96	0.0098
batt_tempC_end	0.49	5.87	0.0166
batt_mAh_charger	0.26	2.08	0.1678
batt_amps_peak	0.79	22.58	<0.0001
batt_amps_average	0.17	1.24	0.3241

Table 4.2 referenced the basic or simple statistical measurements recorded from the experiment test results. Consistent with the analysis of variance results, it could be seen that the peak battery amperage was reduced by 2.22 A or 13.4%, peak temperatures of the battery were reduced by 1.7°C or 5.0%, and ending battery temperature reduced by 1.3°C or 4.0%.

Table 4.2. Simple statistics of the experimental test results.

Response Variable	$\bar{x}$	S	Min	Max
main_volts_end	11.22	0.006	11.20	11.22
batt_tempC_peak	33.1	0.462	32.0	33.7
batt_tempC_end	32.2	0.435	31.4	32.7
batt_mAh_charger	948	8.683	935	961
batt_amps_peak	15.39	0.691	14.36	16.58
batt_amps_average	11.41	0.241	11.11	11.91

4.1.2 Correlation Matrix

Using the SAS 9.4 software, all individual response variables were combined into a visual correlation matrix. The matrix allowed for the observation of unknown correlations and interactions, frequently used for data analytics. Figure 4.1 showed the resulting matrix. The six individual response variables were carried over from the analysis of variance test and plotted along the diagonal of the matrix. All data points were differentiated by their associated test configuration, which symbol was ∘ for battery only, + for 20F5S1P, and x for 80F5S1P.

Closely studying each plot revealed distinct relationships for each variable. A strong correlation can be seen between batt_tempC_peak and batt_tempC_end, as the data points are grouped closely together. The correlation would be expected, as both variables represent the same measurement, just different points in the test.

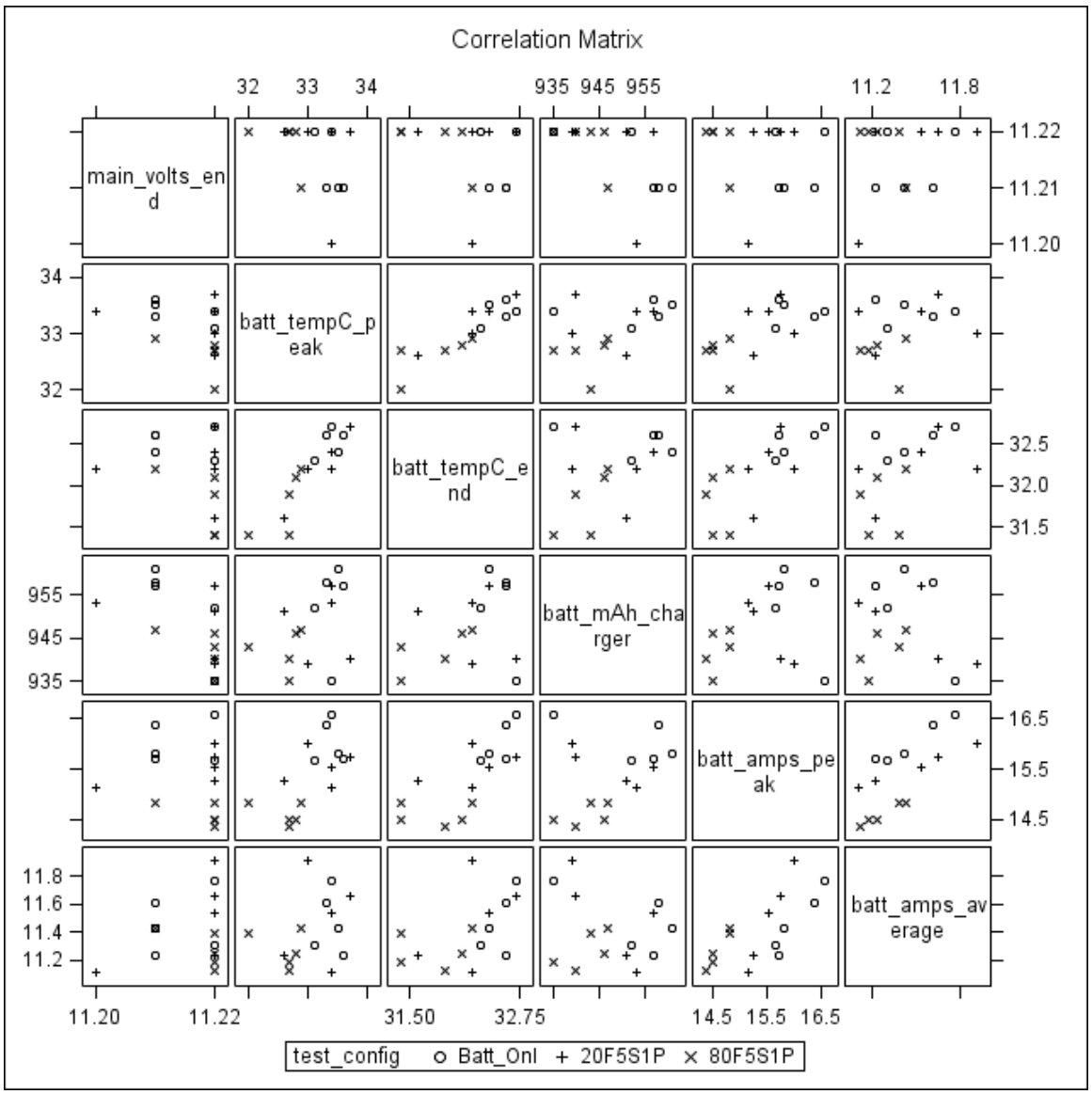

Figure 4.1. Correlation matrix of individual response variables with respect to test configuration. Matrix developed with SAS 9.4.

4.1.3 Visual Comparison of Test Configurations

The proceeding plots were used to help support and validate the experimental results.

4.1.3.1 Check of Standard Deviation for Output Current

A check of standard deviation for the output current was investigated for all 15 observations. The experimental results relied on the fact that the load could be consistently repeated across the 15 tests and the standard deviation checked for error of repeatability.

Referencing Figure 4.2, it could be seen the average standard deviation of current between tests was ±0.047 A and maximum standard deviation was ±0.078 A. For the purpose of the study, the deviation was found to be acceptable.

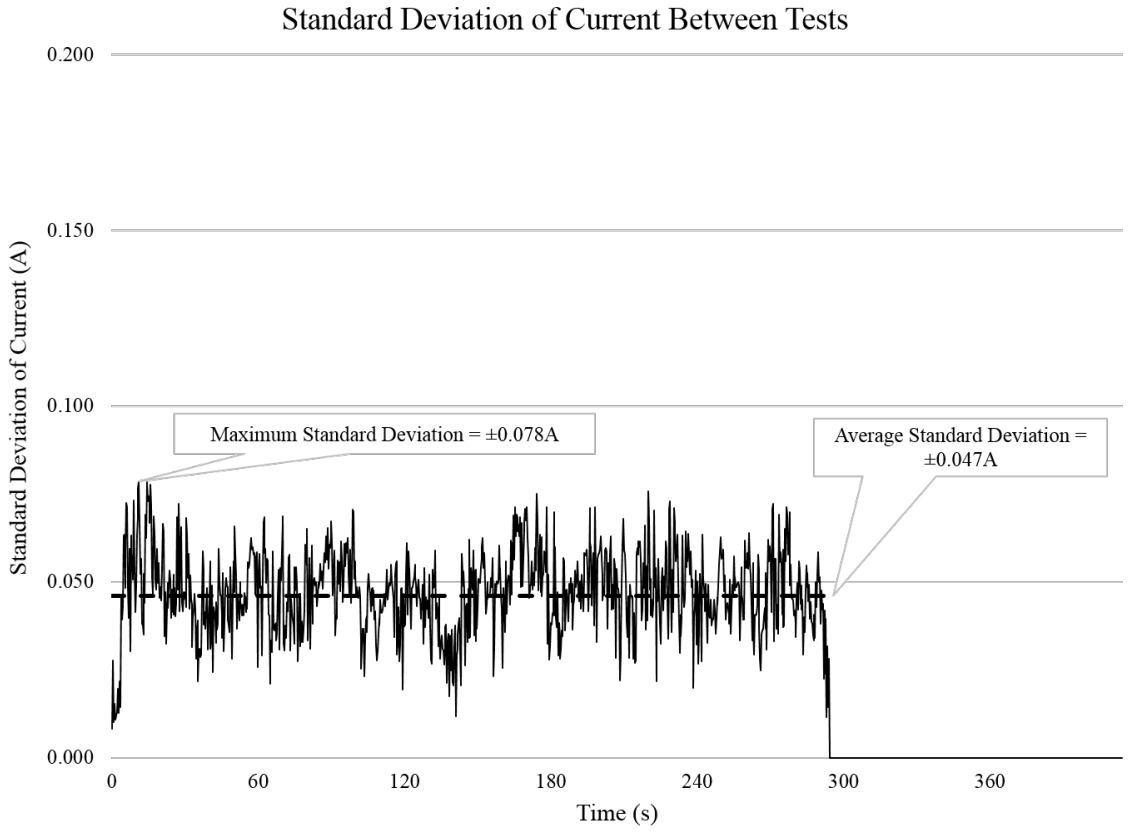

Figure 4.2. Standard deviation of current between experimental tests. Plot developed with Microsoft Excel 2016.

4.1.3.2 Battery Only vs 80F5S1P HESS Configuration

The statistical analysis pointed to a significant reduction in peak battery current. The resulting output plots for the current draw on the battery were pulled for two different

tests for comparison. Test 61 (battery only configuration) and test 73 (80F5S1P HESS configuration) were used for the comparison and were shown in Figures 4.3 and 4.4.

Comparing the two output plots revealed a distinct smoothing of the battery output current when the 80F5S1P HESS configuration was present. The maximum current on the battery decreased by over 1 A. Figures 4.5 and 4.6 on the following page validated that the current draw was nearly the same between the two tests. Matlab R2017a was used to generate the battery and main current validation plots.

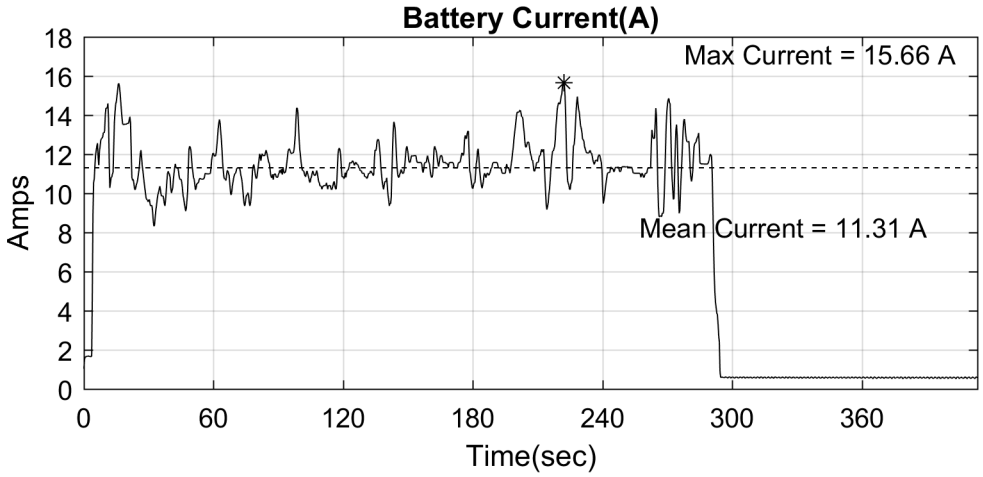

Figure 4.3. Battery current profile for battery only configuration in test number 61.

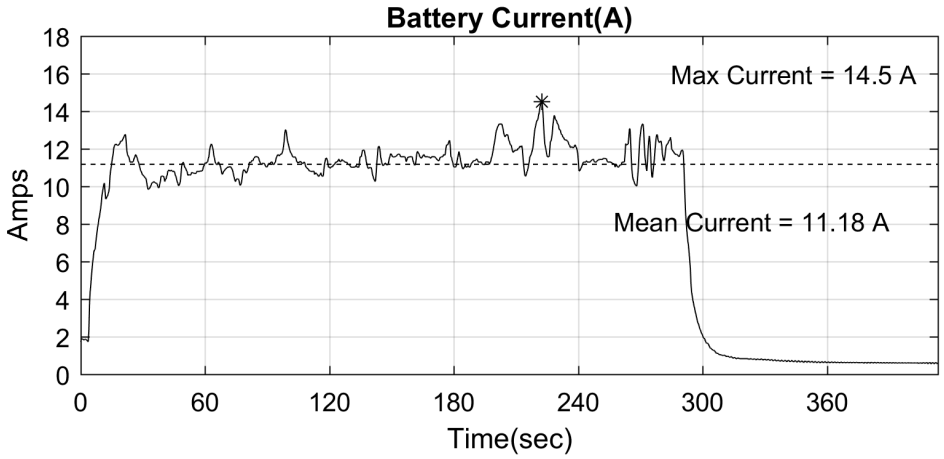

Figure 4.4. Battery current profile for 80F5S1P HESS configuration in test number 73.

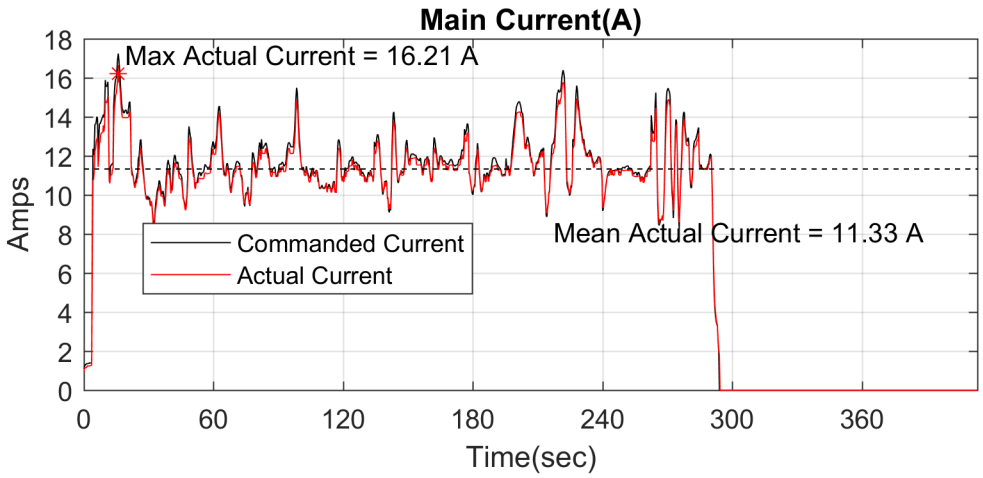

Figure 4.5. Main current profile for battery only configuration in test number 61.

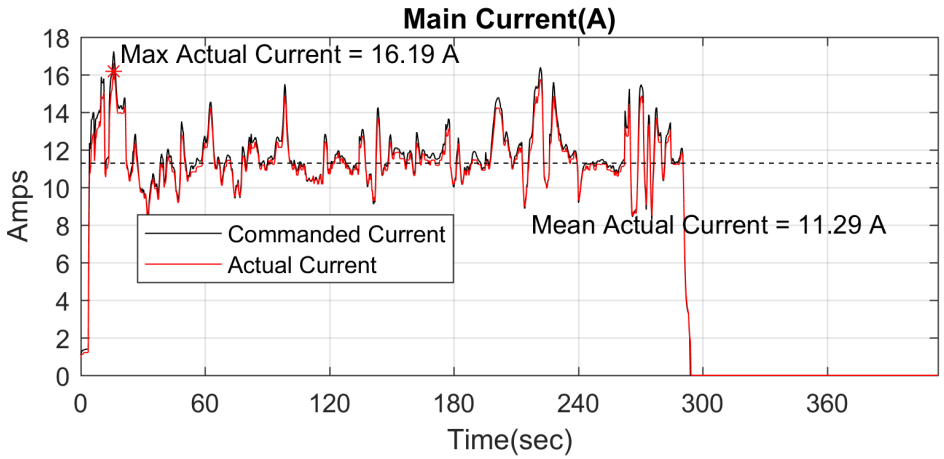

Figure 4.6. Main current profile for 80F5S1P HESS configuration in test number 73.

4.2 Simulation Results

The following section contained the results of the simulation test. The results were derived using the simulation model and defined parameters as outlined for Chapter 3.

Table 4.3 contains a summary of the entire simulation tests results. Identical parameters were measured from the experimental test. The effects of ESR were further investigated by adding two new test configurations. The two new configurations added were the 100F1S1P and 400F1S1P supercapacitor cells. These particular supercapacitors

were based off the same supercapacitors used in the 5S1P arrays, except they only had one capacitor in series instead of five capacitors. Adding the two configurations also assumed the supercapacitor voltage limitation would also be met with some type of a buck/boost converter.

Table 4.3. Complete summary of the simulation test results.

	Simulated Test Configuration				
Parameter	Battery Only	20F5S1P	80F5S1P	100F1S1P	400F1S1P
Total Capacitance (F)	-	20	80	100	400
ESR(Ω)	-	0.0600	0.0110	0.0120	0.0022
Main Voltage Start	12.50	12.56	12.60	12.60	12.61
Main Voltage End	11.54	11.55	11.55	11.55	11.59
Battery TempC Peak	36.4	36.2	35.9	35.7	34.1
Battery TempC End	35.6	35.5	35.2	35.1	33.8
Battery mAh	945	939	922	915	831
Battery Amps Peak	17.24	15.66	14.16	13.91	12.68
Battery Amps Average	11.56	11.48	11.18	11.06	9.39
Battery Ending SOC(%)	27.3	27.8	29.1	29.6	36.1

Consistent with the experimental results, the simulation showed there was an overall decrease in battery amperage and battery temperature. Contrary to the experiment, the simulation results also showed a 2.4% decrease in battery milliamp-hours or energy consumption between the battery and 80F5S1P HESS. This particular result was surprisingly different than what the experimental results showed for energy consumption.

CHAPTER 5. SUMMARY, CONCLUSION, AND RECOMMENDATION

Chapter 5 concluded and summarized the results found from the experiment and simulation based test results. The proceeding section on HESS applicability interpreted the test results found and analyzed the advantages and limitations provided by the HESS configuration. Following the section on applicability was an overview and discussion of the documented weight and volume of each component tested. Finally, the future work, research, and recommendations related to HESS design were discussed.

5.1 Applicability of HESS to a UAV

The following sections discuss and interpret the results found in both experiment and simulation tests of the HESS system as applied to a UAV application. The HESS system provided specific advantages to run time and battery life and those benefits were discussed. Proper sizing and design optimization of the energy storage system to achieve those benefits were discussed as well. Finally, limitations of HESS based on size and weight were addressed.

5.1.1 Experimental Results Interpretation

The overall results of the experiment proved significant advantages to battery performance using a passive HESS. Specifically, decreases for battery peak current and battery peak and ending temperatures were seen. Referencing Table 4.2 results from Chapter 4, the peak battery amperage was reduced by 2.22 A or 13.4%. Peak temperatures of the battery were reduced by 1.7°C or 5.0% and ending battery temperature reduced by 1.3°C or 4.0%.

Unlike the simulation results, no significance was found for battery energy consumption or ending voltage. The simulation results showed a differential SOC gain of 1.8% or SOC percent difference of 6.6% was possible using the 80F5S1P configuration over just the battery. The difference was attributed to a combination of possible I^2R losses in

the charging operation as well as the difference in the experimental batteries and simulation batteries internal resistance value.

Ending voltages stayed the same for the experiment, which correlated with the fact that energy consumption was not reduced. Compared to the simulation results, only a slight increase in ending voltage was seen.

5.1.2 Simulation Results Interpretation

A percent comparison was done using the simulation based results to compare different levels of HESS configurations against the battery by itself. Table 5.1 contained the results of this comparison.

Significant advantages to overall battery performance could be seen when using the 400F1S1P HESS configuration over the battery by itself. The low ESR and high capacitance made this particular configuration very reactive. Not accounting for conversion losses, the peak battery amperage was reduced by 26.5%. The peak temperature was also reduced by -6.3%, and the ending SOC% increased by 32.2% based on a percent difference calculation. Looking at the pure difference in the two, SOC% values showed an increase of 8.8%. The 8.8% increase for SOC% represented a fair and conservative comparison and was used to further quantify theoretical performance improvements.

A limitation to the 100F1S1P and 400F1S1P supercapacitor configurations was for the need of voltage conversion. Voltage conversion would require semi-active and active control methods via a buck/boost converter. The efficiency loss due to the need for a buck/boost converter (typically 95% efficient) was not factored into the 100F1S1P and 400F1S1P results.

The contents in Table 5.2 were recorded values of the original flight translational velocity, distance traveled, and total flight time. The load profile from this flight data was used as the basis of the experimental and simulation tests. Baseline comparisons of the original flight data to simulation values were done to show the new theoretical performance of the UAV using the HESS system. The results of those comparisons are in Table 5.3.

Table 5.1. Simulation based comparison of battery only to individual HESS test configurations.

	Simulated Test Configuration			
% Comparison to Battery Only	20F5S1P	80F5S1P	100F1S1P	400F1S1P
Main Volts at End of Test	+0.1%	+0.1%	+0.1%	+0.4%
Reduction in Peak Battery Temp	-0.5%	-1.4%	-1.9%	-6.3%
Reduction in Ending Battery Temp	-0.3%	-1.1%	-1.4%	-5.1%
Reduction in Battery mAh Consumption	-0.6%	-2.4%	-3.2%	-12.1%
Reduction in Battery Amperage Peak	-9.2%	-17.9%	-19.3%	-26.5%
Reduction in Battery Amperage Average	-0.7%	-3.3%	-4.3%	-18.7%
Increase in Ending Battery SOC (%Diff)	+1.8%	+6.6%	+8.4%	+32.2%
Increase in Ending Battery SOC (Delta)	+0.5%	+1.8%	+2.3%	+8.8%

Table 5.2. Recorded DJI F450 flight log data for comparison of performance with HESS.

Parameter	Recorded Value
Avg. Translational Velocity (m/s)	5
Total Distance Traveled (m)	1240
Total Flight Time (s)	293

Table 5.3. Theoretical performance improvements based on simulation results.

	Simulated Test Configuration			
Parameter	20F5S1P	80F5S1P	100F1S1P	400F1S1P
Run Time Extension (s)				
(Based on Delta SOC% Increase)	1.5	5.3	6.7	25.8
Increase in Distance Traveled (m)	7.3	26.4	33.7	128.9
% Increase in Distance Traveled	+0.6%	+2.1%	+2.7%	+10.4%

5.1.3 Comparison of Experiment to Simulation Results

The simulation based results showed a peak battery amperage reduction of 17.9% while the experimental results showed a reduction of 13.4%. The difference could be attributed to the internal resistance differences between experiment and simulation batteries. The simulation based battery showed an internal resistance of 85 mΩ, which was higher than the 13 mΩ internal resistance of the experimental battery. For the experimental battery, less load was able to be shared and hence, less peak amps were reduced.

The experimental results showed more significant reduction in battery temperature as well. The experiment showed a reduction of peak and ending battery temperatures of 5.0% and 4.0%, while the simulation showed only a reduction of 1.4% and 1.1%. The simulation ambient temperature was set at 22°C, so this could have attributed to less

significant temperature reduction. Different thermodynamic properties between the simulation and experiment could also have been a significant factor in this difference.

5.1.4 Advantages to Run Time Extension

The results from the simulation test for the 400F1S1P configuration showed a run time extension of 25.8 s would be possible. Based on original flight log data, this would have allowed the UAV to travel over 10% farther than with just the battery alone.

5.1.5 Advantages to Battery Life

As cited by the work of Root (2011), excessive heat build-up in the battery is related to the internal resistance and the I^2R loss associated with increasing resistance. The battery would operate more efficiently and cooler by decreasing the peak currents exposed to it. Specifically, for energy dense lithium batteries, this would slow the battery aging process and allow operation at a much safer temperature.

As proven in the experiment and simulation results, this could be done by implementing a parallel battery supercapacitor configuration. The exact life extension factor was not quantified in this work but could be obtained in future simulation work.

5.1.6 Equivalent Series Resistance

Equivalent series resistance (ESR) was found to be a major performance factor. The lower the ESR value of the capacitor bank, the more reactive and efficient the capacitor can be to help filter the pulsed current load. The conclusion coincided with the findings of Dougal et al. (2002) and Chuan et al. (2012). One of the main reasons the 20F5S1P and 80F5S1P supercapacitor configurations failed to give higher performance in comparison to the simulated 100F1S1P and 400F1S1P supercapacitor configurations was due to the summation of the individual ESR values, as defined in Equation 3.3.

The low maximum voltage rating of the individual supercapacitor cells limited applications to voltages lower than the maximum rating. Adding the supercapacitors in

series increased this maximum voltage rating, but consequently increased the ESR value as well as lowered the capacitance value.

5.1.7 Pulse Frequency and Duty Cycle

For the HESS system to work, the load must have a cyclic or pulsed pattern. Specifically, the frequency and duty cycle of the load profile could be used to quantify the gain of the HESS system, as described in Equation 2.2 and the work of Dougal et al. (2002). The capacitor only took part of the load when a voltage difference was present between the capacitor and source, so as the duty cycle approached one, the capacitor could no longer provide benefit to the system. The conclusion again coincided with the work found by Dougal et al. (2002) and Chuan et al. (2012).

5.1.8 Passive vs Active HESS

As tested in both the experiment and simulation tests, the passive HESS system was simple to implement and provided proven benefits of reducing battery peak amperage and battery temperature. A limit to the passive HESS was the rated supercapacitor voltage and the need to put the supercapacitors in series to increase the voltage rating. This caused significant loss in the benefits of the supercapacitor.

The active HESS system required voltage conversion using a buck/boost converter to obtain the needed voltage levels. The active HESS allowed the advantage of much lower ESR and increased capacitance values, but the losses due to converter efficiency must be accounted for. The simulation results of the 100F1S1P and 400F1S1P tests were based on the use of voltage conversion to meet the maximum voltage rating of the capacitors. If the voltage limitation of the supercapacitor could have been increased, the active control system would not be necessary.

5.1.9 Weight and Volume Comparison

One important aspect to understanding and gaging UAV performance was the documentation of weight and volume. Adding the experiment and simulation based HESS configurations to the UAV would require reassessment of design parameters to ensure adequate flight performance.

5.1.9.1 Weight

Power to weight ratio of the UAV has an impact in terms of performance factors of maneuverability and efficiency. Extra weight on board would have to be accounted for and the payload capacity would be subsequently limited. The impact was not measured in the experimental and simulation based results due to the need for further in flight testing. Tables 5.4 and 5.5 below documented the mass of the MHQ250, DJI F450, and battery for comparison. The load profile used for the experiment was based of flight data for the DJI F450.

Table 5.4. Total weight calculation of MHQ250 Drone.

Component	Mass(g)
MHQ250 Drone	509
1300 mAh Battery	112
Total Mass	= 621

Table 5.5. Total estimated weight calculation of DJI F450 Drone.

Component	Mass(g)
DJI F450 Drone	700*
1300 mAh Battery	112
Estimated Total Mass	= 812

*Note: Estimated Based on Specified
Takeoff Weight from Manufacturer (800-1600g)

Table 5.6 summarized the percent of total weight of each energy storage component in comparison to the weight of the UAV with only the battery. The added weight of the 80F5S1P would be within the acceptable weight for the DJI F450 but would also limit

payload capacity. The purposely built supercapacitor arrays were not optimized for weight but for testing purposes. Weight could be reduced for future designs.

Table 5.6. Individual weight and percent of total weight for energy storage components.

Component	Mass(g)	%Total(MHQ250)	%Total(DJI F450)
1300 mAh Battery	112	18.0%	13.7%
20F5S1P Supercapacitor Array	185	29.8%	22.8%
80F5S1P Supercapacitor Array	546	87.9%	67.2%

5.1.9.2 Volume

Volume was another important design aspect in overall UAV design and HESS applicability. Table 5.7 showed the documented dimensions for each energy storage component. The 80F5S1P was considerably larger in comparison to the battery. Adequate space in the UAV would be required for the supercapacitors. Custom supercapacitor array configurations could be used to help conserve space in highly constrained designs.

Table 5.7. Volume of energy storage components.

Component	Height (mm)	Length (mm)	Width (mm)
1300 mAh Battery	20.5	72.2	35.0
20F5S1P Supercapacitor Array	73.0	127.0	38.1
80F5S1P Supercapacitor Array	95.3	186.7	57.2

5.2 Future Work and Recommendation

Future work in HESS design would entail the research of unique ways to address the voltage limitations of the supercapacitor cells, subsequently lowering the ESR values. Simplification of the HESS design is key and solving the voltage limitation problem would lead to great performance enhancements.

The important next step to future research in HESS design validation would be incorporating actual in-flight testing with the HESS configurations.

The recommendation derived from this study is for further optimization, bench testing, and in-flight testing of the HESS. Conclusive results and statistical analysis showed

evidence of battery performance enhancement. The optimized HESS will provide significant advantages to commercialized, long range UAV applications.

5.2.1 Real Flight Testing

A purposely designed and built drone could be used as the test bed for further experimental testing and validation of this research. The autonomous flight controller would allow the same flight path to be repeatedly flown. The required system data could subsequently be recorded and collected for further analysis. Impacts to overall flight performance, such as maneuverability and payload capacity, could also be analyzed. Examining other UAV designs is an opportunity for further flight testing as well.

Variations of UAV aerodynamic designs could have an influence on the cyclic nature of the load. Tilt-rotor and other translational VTOL aircraft have ideal load characteristics for further HESS optimization. Unlike multirotor UAVs with relatively constant load, tilt-rotors have a dynamic load between different flight modes. Vertical takeoff and landing modes draw considerable amounts of power for a short period. Initial flight testing and analysis of load for these designs could highlight potential applicability.

LIST OF REFERENCES

LIST OF REFERENCES

Amazon. (2016). *Amazon prime air.* Retrieved on March 12th, 2017 from https://www.amazon.com/Amazon-Prime-Air/b?node=8037720011.

Borer, N. K., Patterson, M. D., Viken, J. K., Moore, M. D., Clarke, S., Redifer, M. E., ... Osterkamp, P. G. (2016). Design and performance of the nasa sceptor distributed electric propulsion flight demonstrator. In *Aiaa aviation technology, integration, and operations conference* (p. 13-17). Washington, DC: AIAA.

Bose, B. K. (2014). Energy, global warming and impact of power electronics in the present century. In H. Abu-Rub, M. Malinowski, & K. Al-Haddad (Eds.), *Power electronics for renewable energy systems transportation and industrial applications* (p. 1-26). West Sussex, UK: John Wiley & Sons, Ltd.

Business Insider. (2017). *Ups tests drone delivery system (future of shipping report)* (Tech. Rep.). New York, NY: Business Insider Intelligence. Retrieved on February 25th, 2017 from http://www.businessinsider.com/ups-tests-drone-delivery-system-2017-2.

Capata, R., Marino, L., & Sciubba, E. (2014). A hybrid propulsion system for a high-endurance uav: configuration selection, aerodynamic study, and gas turbine bench tests. *Journal of Unmanned Vehicle Systems*, *2*, 16-35. (DOI: 10.1139/juvs-2013-0005)

Chae, J. H., Ng, K. C., & Chen, G. Z. (2010). Nanostructured materials for the construction of asymmetrical supercapacitors. In *Proceedings of the institution of mechanical engineers, part a: Journal of power and energy.* London, UK: Sage.

Chuan, Y., Mi, C., & Zhang, M. (2012, May). Comparative study of a passive hybrid energy storage system using lithium ion battery and ultracapacitor. *World Electric Vehicle Journal*, *5*.

Dougal, R., Liu, S., & White, R. E. (2002, March). Power and life extension of battery-ultracapacitor hybrids. *IEEE Transactions on Components and Packaging Technologies*, *25*(1).

Dubal, D., Ayyad, O., Ruiz, V., & Gomez-Romero, P. (2015, July). Hybrid energy storage: the merging of battery and supercapacitor chemistries. *Royal Society of Chemistry*, *44*, 1777. (DOI: 0.1039/c4cs00266k)

Electropaedia. (2005). *Battery and energy technologies.* Retrieved on November 1st, 2017 from http://www.mpoweruk.com/lithium_failures.htm.

Fawzy, F. (2016, July). *Solar impulse 2: Around the world with zero fuel - cnn.com.* Retrieved on March 12th, 2017 from http://www.cnn.com/2016/07/26/aviation/solar-impulse-world-trip-complete/.

Friedrich, C., & Robertson, P. (2015, January). Hybrid-electric propulsion for aircraft. *Journal of Aircraft*, *52*(1). (DOI: 10.2514/1.C032660)

Grbovic, P. J. (2014). Energy storage technologies and devices. In *Ultra-capacitors in power conversion systems: Applications, analysis and design from theory to practice* (First ed., p. 1-21). West Sussex, UK: John Wiley & Sons, Ltd.

IXYS. (2017). *Ixtn200n10l2 advanced technical information.* Retrieved on November 26th, 2017 from http://ixapps.ixys.com/Datasheet/DS100238(IXTN200N10L2).pdf.

Jensen, H.-C. B., Schaltz, E., Koustrup, S., & Kaer, K. (2013, January). Evaluation of fuel-cell range extender impact on hybrid electrical vehicle performance. *IEEE Transactions on Vehicular Technology*, *62*(1). (DOI: 10.1109/TVT.2012.2218840)

Kerns, J. (2015). *What's the difference between batteries and capacitors?* Retrieved on November 13th, 2017 from http://www.machinedesign.com/batteriespower-supplies/what-s-difference-between-batteries-and-capacitors.

Kurtz, S. (2010). *Pv technology for today and tomorrow.* National Renewable Energy Laboratory. (NREL/PR-520-49176)

Leasure, M., & Nolan, M. S. (2015). *Unmanned aviation systems: The definitive guide.* Fowler, Indiana: eAcademicBooks LLC.

Mi, C., Masrur, M. A., & Gao, D. W. (2011). *Hybrid electric vehicles - principles and applications with practical perspectives.* West Sussex, UK: John Wiley & Sons, Ltd.

Miller, J. R., & Simon, P. (2008, August). Electrochemical capacitors for energy management. *Science Magazine*, *321*. (DOI: 10.1126/science.1158736)

Nickol, C. L., Borer, N. K., Loyselle, P. L., Jones, F. P., Woodham, K., Provenza, A. J., ... Fell, J. S. (2016, January). Overcoming the adoption barrier to electric flight. *AIAA SciTech 2016*, 4-8.

Ozdemir, U., Aktas, Y. O., Vuruskan, A., Dereli, Y., Tarhan, A. F., Demirbag, K., ... Inalhan, G. (2014). Design of a commercial hybrid vtol uav system. *Journal of Intelligent Robot Systems*, *74*, 371-393. (DOI: 10.1007/s10846-013-9900-0)

Pyulog. (2017). *Python module & scripts for ulog files.* Retrieved on November 1st, 2017 from https://github.com/PX4/pyulog. (Computer Software)

Quaternium. (2015). *Hybrix - uav.* Retrieved on February 24th, 2017 from http://www.quaternium.com/portfolio/hybrix-uav/.

Root, M. (2011). *The tab battery book: An indepth guide to construction, design, and use.* New York, NY: Mcgraw Hill.

Sikken, J. (2014, April). *Jasper's electronic load r1.* Retrieved on September 18th, 2017 from http://jasper.sikken.nl/electronicload/index.html.

Solar Impulse. (n.d.). *Adventure.* Retrieved on February 27th, 2017 from www.solarimpulse.com/adventure.

Solar Impulse. (2016, March). *Solar impulse 2 undertakes a maintenance flight in hawaii.* Retrieved on January 27th, 2018 from https://www.flickr.com/photos/solarimpulse/26408079295/in/photostream/.

Sparkfun. (n.d.). *Mcp4725 digital to analog converter hookup guide.* Retrieved on September 27th, 2017 from https://tinyurl.com/ycuea2t6.

Thingiverse.com. (2014). *Hovership mhq2.* Retrieved on June 1st, 2017 from https://www.thingiverse.com/thing:511668.

Uber. (2016). *Fast-forwarding to a future of on-demand urban air transportation.* Retrieved on February 15th, 2017 from https://www.uber.com/elevate.pdf. San Francisco, CA.

U.S. Department of Defense. (2013). *Unmanned systems integrated roadmap fy2013-2038* (Tech. Rep.). Washington, DC: U.S. Department of Defense. (Reference Number: 14-S-0553)

X. (n.d.). *Project wing if we all had access to the sky?* Retrieved on March 12th, 2017 from www.x.company/wing.

Yang, H., Kannappan, S., Pandian, A. S., Jang, J.-H., Lee, Y. S., & Lu, W. (2013). *Achieving both high power and energy density in electrochemical supercapacitors with nanoporous graphene materials.* (Cornell University Library, Condensed Matter, Material Science Archive)

Yeair. (n.d.). *Overview.* Retrieved on March 12th, 2017 from https://yeair.de/.

Zimmermann, T., Keil, P., Hofmann, M., Horsche, M. F., Pichlmaier, S., & Jossen, A. (2016). Review of system topologies for hybrid electrical energy storage systems. *Journal of Energy Storage*, *8*(3), 78-90.

APPENDICES

CHAPTER A. CIRCUIT DIAGRAMS

A.1 Electronic Load Circuit Diagram

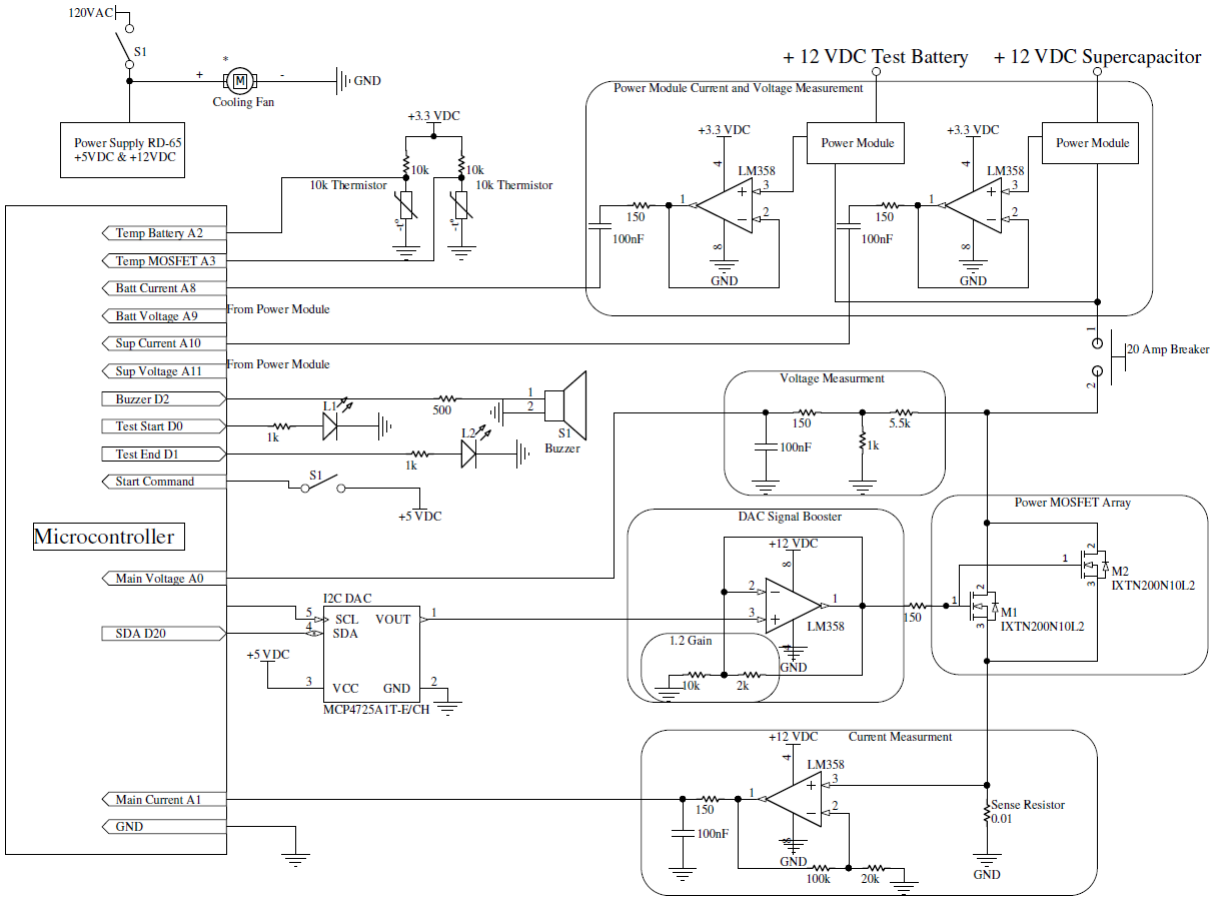

Figure A.1. Electronic load circuit developed for discharge testing of the HESS. The circuit design was conceptually based off the work of Sikken (2014) and was scaled to take a much higher load via the use of paralleled MOSFETs. CircuitMaker 1.3 was used for creation of the circuit diagram.

CHAPTER B. SAMPLE PROGRAMMING CODE REFERENCE

B.1 Electronic Load Tester

B.2 Matlab R2017a - Post-Processing Code

B.3 Matlab R2017a - Simulation Code

```
if (startState == HIGH) {

   timeCount = 0;
   Serial.println("Data logging begin;");
   Serial.println("Time,GateVoltage,MainCurrent,MainVoltage,BatteryCurrent,BatteryVoltage,SupCurrent,SupVoltage,TempCMOSFET,TempCBatt");
   startState = LOW;
   delay(1000);
   myFile = SD.open(myLogFile, FILE_WRITE);//open SD card log file to begin data logging
   i = 0;
   while (startState == LOW) {
     digitalWrite(ledStartpin, HIGH);
     for (i == 0;i<(myCount/6);i++){//reading back array values one-by-one and writing them to SD file
         buttonDebounce();//keep track of start stop button in for loop
         if (startState == HIGH ) {
           commandOff();//call function to turn DAC output to zero
           Serial.println("Stop button pushed. Data logging stops and output to gate set to zero.");
           Serial.println("Press start stop button to start test over.");
           startState = LOW;
           delay(1000);
          return;
           }
          else{
           valVolts = Array[i];
           calculateTemp();
           currentSet(valVolts);
           calculateMainPwr();
           calculateBatt();
           calculateCap();
           String dataString = String(timeCount,1) + "," + String(valGate) + "," + String(mainCurrent,2) + "," + String(mainVoltage,2)
           + "," + String(currentBatt1,2) + "," + String(voltageBatt1,2) + "," + String(currentCap1,2) + "," + String(voltageCap1,2) + "," +
           String(temp1C,1) + "," + String(temp2C,1);
           Serial.println(dataString);
           myFile.println(dataString);
           myFile.close();
           delay(300);//3hz cycle rate
           timeCount = timeCount + 0.3;
```

Figure B.1. Main programming loop for electronic load tester. Part of the code was sourced from Arduino 1.8.4 IDE examples (https://www.arduino.cc/).

```
void currentSet (float valVolts){ //valVolts are read from the array file one by one and fed into this
   if (temp1C < 20) { //if the temperature is less 20°C then don't correct the gate voltage
      correctedVolts = valVolts;
   }
   else {
   correctedVolts = valVolts + (-0.004*(temp1C-20));
   //temperature correction calculation based on rising MOSFET temperature **old coefficient 0.0038**
   }
   valSteps = correctedVolts/1.2*(4095/ref5v);
   // Divide by 1.2 to account for the op amp gain and convert gate voltage to 12 bit steps for the DAC
   valGate = valSteps*((ref5v/4095)*1.2);

    Wire.beginTransmission(MCP4725_ADDR);//initialize DAC transfer
    Wire.write(64);//command to update DAC
    Wire.write(valSteps/16); // the 8 most significant bits
    Wire.write((valSteps % 16) << 4); //the 4 least significant bits
    Wire.endTransmission();
}
```

Figure B.2. Output current set code using I2C communication. Part of this code was sourced from the MCP4725 technical documentation (Sparkfun, n.d.).

```
% Clear all existing variables and close all open figures
clear all;
close all;
clc;

% Open an excel spreadsheet containing the specific current profile being
% tested

CurrentPlot = xlsread('CurrentPlot_2m_rest','A2:B1380');
%This brings in the current profile data to load into the simulink model
CommandedCurrent = CurrentPlot;
filename = 'Test75_20F_2018_1_5.xlsx';
ExperimentalDataTable = {
readtable(filename,'Range','A1:J1380','ReadVariableNames',true)};

BatteryCapacity = 4680;
BatterySOCint = 100; %Battery starting SOC
sim('HESS_ExperimentSOCEstimater');

% SupercapCapacity = 135;
% SupercapSOCint = 93; %Battery starting SOC
% sim('HESS_SupercapSOCEstimater');

cEnergyMain = cumsum(ExperimentalDataTable.MainCurrent*0.3);
cEnergyActual = cumsum(CurrentPlot(:,2)*0.3);
cEnergyBattery = cumsum(ExperimentalDataTable.BatteryCurrent*0.3);
cEnergySup = cumsum(ExperimentalDataTable.SupCurrent*0.3);

% Run the script to create a figure of the simulation
HESSExperimentalFigure;
```

Figure B.3. Sample Matlab R2017a code used for post-processing of experimental data.

```
% Clear all existing variables and close all open figures
clear all;
close all;
clc;
% Open an excel spreadsheet containing the specific current profile being
% tested
CurrentPlot = xlsread('CurrentPlot_2m_rest','A1:B1081');
%This brings in the current profile data to load into the simulink model
% Declare variables:
capStartVoltage = 12.6;
ratedVoltage = 2.7;
% Configuration topology:
numCapSeries = 1;
numCapParallel = 1;
% IC  Supercapacitor Parameters:
%capacitance = 100;
%ESR = 0.012;
% AVX SCCY68B407SSBLE Supercapacitor Parameters:
capacitance = 400;
ESR = 0.0022;

configurationVoltage = ratedVoltage * numCapSeries;

if (configurationVoltage < 12)
    configurationVoltage = 17
end

configurationCapacitance = (capacitance/numCapSeries) * numCapParallel;
configurationESR = ESR * numCapSeries;

% Run the simulation
sim('HESS_Model_2017_11_16');
% Run the script to create a figure of the simulation
HESSFigureModified;
```

Figure B.4. Sample Matlab R2017a code used for simulation.

CHAPTER C. LOG OF EXPERIMENTAL DATA

C.1 Test Log Data

C.2 Sample of Raw Test Data

Table C.1. Test log of recorded experimental data.

	Test Number														
Parameter	61	62	63	64	65	66	67	68	69	70	71	72	73	74	75
Date							-1/5/17-								1/6/17
Time	10:45	10:57	11:13	11:25	12:22	12:50	13:12	16:15	16:33	16:49	18:12	18:32	21:17	21:25	9:21
TConfig	C	A	B	A	C	B	C	B	A	B	A	C	B	C	A
BattPack#	1A	2A	3A	4A	5A	1A	2A	3A	4A	5A	1A	2A	3A	4A	5A
CapV@Start	-	12.3	11.7	12.2	-	12.2	-	12.2	12.2	12.2	12.2	-	12.1	-	12.1
BattV@Start	12.56	12.58	12.57	12.58	12.57	-	12.56	12.51	12.51	12.51	12.51	12.51	12.51	-	12.50
BattSOC%@ Start	99	99	99	99	99	-	99	98	98	98	98	98	98	-	97
BattV@End	11.26	11.25	11.23	11.25	11.23	11.26	11.23	11.25	11.24	11.24	11.25	11.23	11.24	11.23	11.23
BattSOC%@ End	15	15	15	15	15	15	15	15	15	15	15	15	15	15	15
MainV@Start	12.49	12.49	12.42	12.47	12.51	12.42	12.49	12.43	12.43	12.43	12.43	12.43	12.36	12.43	12.43
MainV@End	11.22	11.22	11.21	11.22	11.22	11.22	11.21	11.22	11.22	11.22	11.22	11.21	11.22	11.21	11.20
BattTempC Peak	33.1	33.7	32.9	33.0	33.4	32.0	33.5	32.7	33.4	32.8	32.6	33.6	32.7	33.3	33.4
BattTempC End	32.3	32.7	32.2	32.2	32.7	31.4	32.4	31.9	32.4	32.1	31.6	32.6	31.4	32.6	32.2
BattmAh Charger	952	940	947	939	935	943	961	940	957	946	951	957	935	958	953
BattmAh Matlab	943.8	973.6	967.5	935.8	980.2	959.8	952.7	938.5	963.9	947.4	939.4	936.7	942.2	968.1	929.3
BattAmpsPeak	15.66	15.74	14.82	16.02	16.58	14.82	15.81	14.36	15.54	14.50	15.26	15.71	14.50	16.39	15.14
BattAmps Average	11.31	11.65	11.43	11.91	11.76	11.39	11.42	11.12	11.53	11.24	11.23	11.23	11.18	11.61	11.11

Table C.3. Sample raw experimental data from test 61.

Time_s	GateVolts	MainAmps	MainVolt	BattAmps	BattVolts	SupAmps	SupVolts	TempCMOS	TempCBatt
0.0	3.68	0.95	12.49	1.04	12.45	0.00	12.27	21.3	20.7
0.3	3.70	1.13	12.47	1.51	12.43	0.00	12.24	21.3	20.7
0.6	3.71	1.15	12.44	1.63	12.41	0.00	12.23	21.2	20.7
0.9	3.71	1.15	12.43	1.66	12.40	0.00	12.21	21.2	20.7
1.2	3.71	1.15	12.43	1.66	12.40	0.00	12.22	21.2	20.7
1.5	3.72	1.23	12.43	1.66	12.39	0.00	12.21	21.2	20.7
1.8	3.72	1.25	12.43	1.68	12.40	0.00	12.21	21.2	20.7
2.1	3.72	1.23	12.43	1.68	12.40	0.00	12.21	21.2	20.7
2.4	3.72	1.26	12.43	1.68	12.39	0.00	12.20	21.2	20.7
2.7	3.72	1.23	12.43	1.66	12.39	0.00	12.20	21.2	20.7
3.0	3.72	1.27	12.43	1.66	12.39	0.00	12.20	21.2	20.7
3.3	3.72	1.26	12.43	1.66	12.39	0.00	12.20	21.2	20.7
3.6	3.72	1.27	12.43	1.66	12.39	0.00	12.20	21.2	20.7
3.9	4.12	6.96	12.06	4.75	11.53	0.00	11.16	21.2	20.7
4.2	4.26	10.75	11.74	8.96	10.86	0.00	10.38	21.2	20.7
4.5	4.25	10.79	11.71	10.54	10.79	0.00	10.34	21.2	20.7
4.8	4.26	11.23	11.67	10.75	10.74	0.00	10.25	21.2	20.7
5.1	4.29	12.24	11.58	11.43	10.58	0.00	10.07	21.2	20.7
5.4	4.29	12.38	11.56	11.93	10.53	0.00	10.03	21.3	20.7
5.7	4.30	12.74	11.50	12.21	10.50	0.00	9.96	21.2	20.7
6.0	4.30	12.85	11.48	12.41	10.47	0.00	9.94	21.3	20.7
6.3	4.30	12.98	11.48	12.57	10.45	0.00	9.93	21.3	20.7
6.6	4.25	11.44	11.56	11.82	10.68	0.00	10.20	21.3	20.7
6.9	4.27	11.95	11.50	11.44	10.59	0.00	10.09	21.3	20.7
7.2	4.29	12.66	11.45	12.14	10.50	0.00	9.98	21.3	20.7
7.5	4.29	12.73	11.43	12.41	10.49	0.00	9.96	21.4	20.7
7.8	4.30	13.10	11.39	12.71	10.43	0.00	9.88	21.4	20.7